WIRELESS HEALTH MONITORING AND IMPROVEMENT SYSTEM FOR WIND TURBINES

by

SURATSAVADEE KOONLABOON KORKUA

Presented to the Faculty of the Graduate School of

The University of Texas at Arlington in Partial Fulfillment

of the Requirements

for the Degree of

DOCTOR OF PHILOSOPHY

THE UNIVERSITY OF TEXAS AT ARLINGTON

December 2011

Copyright © by Suratsavadee Koonlaboon Korkua 2011

All Rights Reserved

ACKNOWLEDGEMENTS

I would like to express deep gratitude to my supervisor professor, Dr. Wei-Jen Lee, for his guidance, encouragement, patience, and support throughout the development of this dissertation and my academic program. In addition to research skills, I have also learned the following traits from Dr. Wei-Jen Lee: self-discipline, diligence, continual self-improving, and the importance of enjoying research and life. He was and always will be a role model throughout my life.

I would like to extend my appreciation to Dr. Somboon Sangwongwanich, who guided and directed through my M.S. study and research at Chulalongkorn University, Thailand. Without his support and encouragement, I could not have gone so far in my academic career.

I wish to thank Dr. William E. Dillon, Dr. Rasool Kenarangui, Dr. Soontorn Oraintara and Dr. David A. Wetz for their instruction and for serving on my dissertation committee, providing valuable suggestions and review.

I also want to express appreciation to the Royal Thai Government for financial support and giving me the opportunity to pursue a Ph.D. degree. I also thank all members of Energy Systems Research Center (ESRC) at the University of Texas at Arlington for all their valuable assistance, discussions, and enjoyable association.

Finally, I dedicate my dissertation to my parents for their continuous sacrifices. I am also indebted to my husband and my son for their patience and sacrifice while being so far away from their beloved. I am very grateful to them for their love, encouragement and continuous support.

November 2, 2011

ABSTRACT

WIRELESS HEALTH MONITORING AND IMPROVEMENT SYSTEM FOR WIND TURBINES

Suratsavadee Koonlaboon Korkua, Ph.D.

The University of Texas at Arlington, 2011

Supervising Professor: Wei-Jen Lee

Wind power has become the world's fastest growing renewable energy resource. The world-wide wind power installed capacity has exceeded 120 GW. The United States has set a target of 20% wind-based electricity generation, over 300 GW, by 2030. As wind power is growing towards becoming a major utility source, it is urgent to guarantee the reliable operation of wind power systems. To avoid unexpected equipment failures, the focus in most wind farm is shifting from scheduled preventive maintenance to predictive maintenance. Predictive maintenance by condition-based monitoring of electrical machines is a scientific approach that is becoming a new strategy for maintenance management.

Vibration analysis is also a measurement tool used to identify, predict, and prevent failures in rotating machinery. Implementing vibration analysis will improve the reliability of the machine and lead to better machine efficiency, reducing downtime by eliminating unexpected mechanical or electrical failures. Traditionally, monitoring systems are implemented as in wired systems formed by communication cables and various types of sensors. The cost of installation and maintenance such a system is more expensive than the cost of the sensors themselves.

To overcome the restrictions of wired networks, using wireless system for monitoring is proposed. A wireless sensor network is a new control network that integrates the sensors, and embedded computer, wireless communication, and intelligent processing technology. ZigBee is

a new wireless networking technology with low power, low cost, and short time-delay characteristics. Compared with other similar standards such as Bluetooth, it tends to provide each single device lower complexity and cost. Based on ZigBee network communication technology, the system can deal with the various operating parameters of remote transmission, real-time data collection, and real-time health monitoring systems. Moreover, ZigBee wireless technology enables the identification of the location of each node under the network with several types of positioning algorithms.

This study presents and develops a ZigBee based wireless sensor network for machine health monitoring of induction machines. The three-axis vibration signals obtained from the monitoring system are then processed and analyzed with signal processing techniques. The vibration detection techniques with suitably modified algorithms are used to extract information for an induction machine health diagnostic. The severity level of abnormality and the remaining usable life are also explored.

The goal for this research is not only to monitor the machine health of wind turbine system, but also to develop a control method for doubly-fed induction generators (DFIG) that addresses the issues associated to the rotor imbalance condition of the generator. Rotor imbalance is a mechanical disturbance related problem. It is a condition where there is more weight distributed on one side of a rotating part of the rotor than on the other side. It might be caused by wind wheel unbalances, shaft imbalances, or mechanical looseness. This kind of event will directly cause oscillation on the output signal of the generator such as generated output power, current, and voltage. The proposed control method will improve the performance of the DFIG control system by reducing the oscillation of the generator output and allowing the system to operate during the slightly unbalanced condition. To suppress the vibration and minimize the oscillation of the generated output, in addition to reducing the stresses on the wind turbine, the rotor side inverter controller is designed and tested by way of a digital simulation on the Matlab/Simulink platform.

The wireless health monitoring system for wind turbine based on vibration detection shows the validity and distinct advantages in such a condition based monitoring system. The severity level of rotor imbalance is successfully estimated by using machine vibration analysis. Moreover, the systematic control design of the proposed vibration suppression by means of a rotor side inverter controller is explored and discussed. The real wind speed data of four different cases from the ERCOT system were used as input to test the performance and capabilities of the control scheme. The simulation results of the generator output show the effectiveness of this proposed rotor side inverter controller. It effectively reduces the oscillation of power, current, and torque output of the DFIG wind turbine.

TABLE OF CONTENTS

ACKNOWLEDGEMENTS iii

ABSTRACT iv

LIST OF ILLUSTRATIONS xi

LIST OF TABLES xiv

Chapter Page

1. INTRODUCTION 1

1.1 Health Monitoring System for Wind Turbines: Background and Problems 1

1.2 Wind Turbine Failures and Fault Detection 2

1.3 The Proposed Method 5

1.4 Study Objectives 6

1.5 Synopsis of Chapters 7

2. LITERATURE REVIEW 9

2.1 Present Wind Turbine Condition Monitoring and Fault Diagnosis 9

2.1.1 Gearbox and Bearing 9

2.1.2 Generators 11

2.2 Review Conclusions 12

3. THE PROPOSED WIRELESS HEALTH MONITORING SYSTEM 13

3.1 Condition based Monitoring System for Wind Turbines 13

3.2 Vibration Sensor Equipment 14

3.3 Machine Vibration Analysis 16

3.3.1 Time Domain Approach 17

3.3.1.1 Implementation of Trend Monitoring 18

3.3.1.2 Implementation of Signal Averaging 18
3.3.1.3 Implementation of Root Mean Square 19
3.3.1.4 Implementation of Crest Factor 19
3.3.2 Frequency Domain Approach 20
3.3.2.1 Implementation of Spectrum Analysis 20
3.4 Wireless Network Communication 22
3.4.1 ZigBee/IEEE 802.15.4 Standard 22
3.4.2 ZigBee based System Framework 23
3.4.3 Hardware Design of Node and Base Station 24
3.4.3.1 CC2430 Introduction 24
3.4.3.2 ADXL330 MEMS Accelerometer 25
3.4.3.3 Node 26
3.4.3.4 Base Station 26
3.4.4 Software Design 26
3.4.5 Software Flow 27
4. FAULT DETECTION OF INDUCTION MACHINE UNDER ROTOR IMBALANCE CONDITIONS 30
4.1 Induction Motor under Rotor Imbalance 30
4.2 Effect on Vibration Signature 31
4.3 Validation of Rotor Imbalance Detection 32
4.3.1 The Proposed Wireless Machine Health Monitoring System 32
4.3.2 Experimental Setup 32
4.3.3 Experimental Results 34
4.4 Summary 37
5. OPERATION OF WIND TURBINE SYSTEMS 38
5.1 Overall Control System of DFIG Wind Turbines 39
5.2 Aerodynamic Model 40

5.3 Transmission System 40
5.4 Doubly Fed Induction Generator Model 41
5.5 Wind Turbine Control Level Model 42
5.5.1 Power Controller 42
5.5.2 Speed and Pitch Controller 43
5.6 DFIG Control Level Model 44
5.6.1 Grid Side Converter 44
5.6.2 Conventional Rotor Side Inverter 46
5.7 Summary 48
6. THE PROPOSED ROTOR SIDE INVERTER CONTROLLER 49
6.1 The Proposed Control Structure of the Rotor Side Inverter Controller 49
6.2 Stator Flux Magnitude and Phase Angle Estimation 50
6.3 Oscillating Rotor Current Extraction 50
6.4 Stator Side Current Estimation 51
6.5 Modified Decoupling Voltage Control 53
6.6 Simulation Setup 55
6.7 Simulation Results 56
6.7.1 Constant Wind Speed Event 56
6.7.2 Instantaneous Wind Ramp up Event 59
6.7.3 Instantaneous Wind Ramp down Event 62
6.7.4 Wind Gust Event 65
6.8 Summary 68
7. CONCLUSIONS AND FUTURE RESEARCH 69
7.1 Conclusions 69
7.2 Dissertation Contributions 70
7.3 Possible Future Research 71

APPENDIX

A. SOURCE CODE 73

REFERENCES 93

BIOGRAPHICAL INFORMATION 99

LIST OF ILLUSTRATIONS

Figure Page

1.1 Catastrophic Failure of a Wind Turbine due to Lack of Proper Monitoring System 2

1.2 Annual Hours Lost Caused by Wind Turbine Subassemblies 3

1.3 Diagram of a Wind Turbine with a Two-stage Gearbox 4

3.1 Major Components of Wind Turbine 14

3.2 Common Sensor Configurations for Horizontal Axis Wind Turbine 15

3.3 Block Diagram of the Proposed Severity Detection Technique of Rotor Imbalance 22

3.4 Structure of the Wireless Sensor Network 24

3.5 Hardware Framework 24

3.6 Block Diagram of ADXL330 MEMS Accelerometer 25

3.7 The Frame Format 27

3.8 The Flow Chart of PAN Network Coordinator (left side)
and Data Collection Node(right side) 28

4.1 Rotational Model of Horizontally Mounted Mechanical System under Rotor Imbalance 30

4.2 Schematic Diagram of the Wireless Machine Health Monitoring System 32

4.3 ADXL330 Tri-axial Accelerometer Mounted on the Motor Housing 33

4.4 Flywheel Design used in Rotor Imbalance Test 33

4.5 Example of a Data Collection Node Board (left side) and
a PAN Network Coordinator (right side) 34

4.6 RMS Value of Vibration Signals from Different Imbalance Mass Tests 34

4.7 Three-axis Vibration Spectrum Component Amplitude at
Rotating Frequency from Different Weights of Imbalance Mass 36

4.8 Three-axis Magnitude of Vibration Spectra at Rotating Frequency
Versus the Different Weights of Imbalance Mass 36

4.9 Rotor Imbalance Indicator of Different Levels of Imbalance Severity 37

5.1 Wind Turbine Control System 39

5.2 A Two-Mass Model 40

5.3 Power-Speed Tracking Characteristic 42

5.4 General Electric's Wind Turbine 1.5-77 Series Model 43

5.5 Power-Speed Characteristic of GE' Wind Turbine 1.5-77 Series Model 43

5.6 Wind Turbine Control Level 44

5.7 Schematic Diagram of the Grid Side Converter 44

5.8 Vector Control Structure for Grid Side Converter Controller 46

5.9 Vector Diagram in d-q Reference Frame considering a Field Oriented Control 47

5.10 Vector Control Structure for Conventional Rotor Side Inverter Controller 48

6.1 Proposed Control Structure of Rotor Side Inverter Controller 50

6.2 Frequency Response of the Low Bandwidth Second Order Band-Pass Filter 51

6.3 Simulation Results of Wind Speed (m/s), Generator Speed (p.u.),
Generated Power Output (MW) and Electromechanical Torque (p.u.)
responded on Constant Wind Event 57

6.4 Simulation Results of Generated Power Output (MW)
: Before and After Suppression 57

6.5 Simulation Results of Electromechanical Torque (p.u.)
: Before and After Suppression 58

6.6 Simulation Results of Generated Current Output (p.u.)
and Zoom Versions of Current Output (p.u.): Before and After Suppression 58

6.7 Wind Ramp up Event on February 25th, 2008 59

6.8 Simulation Results of Wind Speed (m/s), Generator Speed (p.u.),
Generated Power Output (MW) and Electromechanical Torque (p.u.)
responded on Wind Ramp up Event 60

6.9 Simulation Results of Generated Power Output (MW)
: Before and After Suppression 60

6.10 Simulation Results of Electromechanical Torque (p.u.)
: Before and After Suppression 61

6.11 Simulation Results of Generated Current Output (p.u.)
and Zoomed Versions of Current Output (p.u.): Before and After Suppression 61

6.12 Wind Ramp down Event on February 28th, 2008 62

6.13 Simulation Results of Wind Speed (m/s), Generator Speed (p.u.),
Generated Power Output (MW) and Electromechanical Torque (p.u.)
responded on Wind Ramp down Event..... 63

6.14 Simulation Results of Generated Power Output (MW)
: Before and After Suppression 63

6.15 Simulation Results of Electromechanical Torque (p.u.)
: Before and After Suppression……. 64

6.16 Simulation Results of Generated Current Output (p.u.) and Zoomed Versions
of Current Output (p.u.) versus Time(s): Before and After Suppression.. 64

6.17 Wind Gust Event on March 4th, 2008 65

6.18 Simulation Results of Wind Speed (m/s), Generator Speed (p.u.),
Generated Power Output (MW) and Electromechanical Torque (p.u.)
responded on Wind Gust Event 66

6.19 Simulation Results of Generated Power Output (MW)
: Before and After Suppression 66

6.20 Simulation Results of Electromechanical Torque (p.u.)
: Before and After Suppression 67

6.21 Simulation Results of Generated Current Output (p.u.)
and Zoomed Versions of Current Output (p.u.): Before and After Suppression.. 67

LIST OF TABLES

Table Page

4.1 Crest Factor of Three-axis Vibration Signals from Different Imbalance Mass Tests 35

6.1 9-MW Wind Farm Parameters in this Study 56

CHAPTER 1

INTRODUCTION

1.1 Health Monitoring System for Wind Turbines: Background and Problems

Wind power has become the world's fastest growing renewable energy resource. The worldwide wind power installed capacity has exceeded 120 GW. The United States has set a target of 20% wind-based electricity generation—over 300 GW—by 2030 [1]. As wind power becomes a major utility source, it is crucial to ensure the reliable operation of these power systems in order to improve both quantity and quality of wind power generation. Wind turbines are subject to different sort of failures. Therefore, before exploring condition monitoring and fault diagnostic methods in wind turbines, the different kinds of failures, as well as their downtime consequences, are reviewed [2-7]. Of course, obtaining reliable power from wind turbine generators, which are complex electromechanical systems, requires high performance monitoring systems.

Analysis of wind farm maintenance costs has shown that up to 40% of the cost can be related to unexpected failures of wind turbine components that then lead to unscheduled corrective maintenance actions [8-9]. Unscheduled corrective maintenance is the most costly type of maintenance, and it is always at high risk for consequential damages resulting in extensive downtimes. To avoid these problems, the focus of most wind farms is shifting to predictive maintenance. Predictive maintenance by condition-based monitoring of electrical machines is a scientific approach that is becoming the new strategy for maintenance management. It is performed before failure, while the corrective maintenance is performed after. Moreover, there are many advantages to this method, such as the full lifetime use of components, low expected downtime, and easy-to-spare part logistics. However, high performance condition based monitoring hardware and software has resulted in higher cost. To

justify the investment and take advantages of predictive maintenance, reliable information about the remaining lifetime of the components is required and appropriate condition threshold values have to be established.

Wind turbine condition-based health monitoring systems collect data from the main components of a wind turbine such as the generator, the gearbox, the main bearing, the shaft and the yaw system. The purpose is to minimize downtime and maintenance cost while increasing energy availability and extending the lifetime service of wind turbine components. An ideal condition monitoring system monitors all the components with a minimum number of sensors. Though wind turbine manufacturers and operators have been working hard to develop advanced condition based monitoring systems in order to evaluate the structural condition of wind turbines and maintain an operational state to enhance the efficiency and prevent the failures, the accident still happens. Figure 1.1shows the consequences of the lack of proper machine health monitoring system of wind turbines. (Available from http://www.flickr.com/photos/canuck01/4709751212/)

Figure 1.1 Catastrophic Failure of a Wind turbine due to Lack of Proper Monitoring System

1.2 Wind Turbine Failures and Fault Detection

A wind turbine consists of thousands of components and is subject to different sorts of failures. Some of them are more frequent than others but in order to compare among them it is necessary to consider the downtime they could force for the whole system. In practice, the resultant economic loss which is directly caused by the downtime of a particular component is the most important industry metric for determining the criticality of a machine component.

In this work, the economic losses caused by wind turbine subassemblies are approximated by the downtimes caused by failures. Figure 1.2 gives the annual average downtimes of major wind turbine subassemblies according to the LWK survey of more than 2000 wind turbines for 11 years [10].

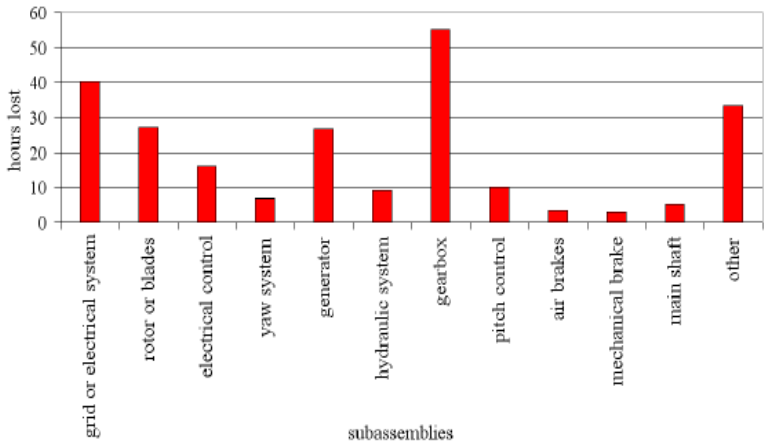

Figure 1.2 Annual Hours Lost Caused by Wind Turbine Subassemblies

From the statistic data shown in Figure 1.2, it is seen that gearbox, grid or electrical system, rotor blade, and generator are ranked the four most critical subassemblies based on annual average downtime; consequently, they should received the highest priority for monitoring due to the high downtime caused by their malfunction. Currently, the commercially available condition monitoring systems have paid much attention to monitoring these subassemblies [11-12]. However, most monitoring systems focus more on detecting electrical faults occurring in generator, grid or electrical system, and electrical control parts such as the converter [13-17]. The most commonly used information for monitoring system includes temperature measurement, lubrication oil analysis, and strain measurement [18-19]. These techniques are valid for detecting local mechanical failures, but they are not so successful in detecting mechanical faults occurring in the gearbox and generator.

For better understanding on mechanical faults in wind turbines and facilitating the explanation of the new vibration based health monitoring strategy proposed in this work, a diagram of a wind turbine with a two-stage gearbox is shown in Figure 1.3 [20].

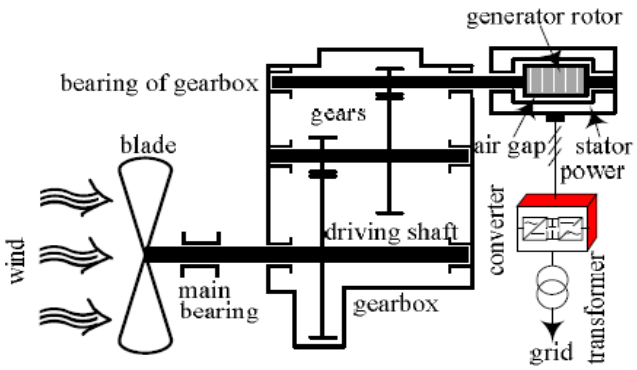

Figure 1.3 Diagram of a Wind Turbine with a Two-stage Gearbox

From Figure 1.3, one can see that wherever mechanical faults occur—whether in the blades, the main bearings, the driving shaft, or the bearings of the gearbox—the energy flow created by the fault travels along the drive train and in the end reaches the generator of the wind turbine. This energy will disturb the air-gap between the rotor and the stator of the generator, producing one or more of the following phenomena: rotor imbalance, unbalances and harmonics in air gap flux, increased torque pulsation, and increased losses and reduction in efficiency. It will also directly affect the output of the generator such as power, current and voltage.

Many approaches and techniques have been explored to investigate techniques for fault detection in electrical machines. Some conventional methods such as Motor Current Signature Analysis (MCSA) with various DSP and signal processing techniques [21-25] have been utilized to search for an accurate machine signature. Since the rotor imbalance is a mechanically related problem, the possibility of an analysis of machine vibrations is obvious. In addition, owing to the increase in economic pressure and the potential consequence due to the vibration problems in electrical machines, a low cost and more reliable method is desirable for

diagnostic studies. This requires a good accelerometer for vibration measurement. Though the technique for detecting electrical faults such as grid voltage unbalance has been explored by other researchers, the mechanical fault and the level of severity have not previously been discussed. Thus, a vibration based detection and diagnostic of rotor imbalance conditions is still needed today. The accelerometer based on MEMS technology is gaining popularity due to low cost, high reliability and low power consumption [26]. It is the ideal component for the proposed health monitoring system.

1.3 The Proposed Method

In this dissertation, in order to detect the rotor fault imbalance condition of wind turbines, the proposed method of vibration monitoring of electrical machine health conditions uses the vibration information collected through a ZigBee based wireless sensor network. Detection techniques using a signal processing technique with suitably modified algorithms is used to extract detailed information to determine machine health condition.

As the first step, the vibration data is fed into the machine analysis to identify the important vibration signature. Based on the vibration spectrum analysis, the RMS value, Crest factor, and spectrum amplitude in the expected rotational frequency range are extracted. The Fast Fourier Transform (FFT) algorithm is used to perform discrete Fourier transform (DFT) for all three-axis vibration signals. The rotor imbalance indicator by using the amplitude of expected frequency components as an indicator of rotor imbalance successfully reveals the severity level of the rotor imbalance condition. The remaining usable life of the machine is also estimated. All techniques mentioned above have been validated and investigated by hardware implementation and experimental results.

Moreover, to improve the quality of wind turbine output and to suppress the vibration on the rotating part of the machine during the rotor imbalance condition, the doubly-fed induction generator (DFIG) wind turbine control system is studied and a new control strategy for the rotor side inverter controller to suppress the power fluctuation due to rotor imbalance of the wind

turbine is also proposed. The current control approach by a vector oriented control (VOC) philosophy in the d-q reference frame is applied. This is useful for reducing the complexity of the DFIG mathematical equation from Park's transformation. Under the wind turbine control level, the oscillating rotor side current is first extracted by frequency-varying low bandwidth band-pass filter. This rotor current is then used to estimate the next sampling stator side current in order to better perform the current control. The stator flux amplitude and phase angle are also estimated during the rotor imbalance condition. Modification of decoupling voltage control makes it possible to obtain the estimated rotor voltage that is needed to inject the desired current into the DFIG via the current-controlled voltage source PWM inverter. This technique reduces the oscillation of wind turbine output by control from the rotor side, which requires lower power injection compared with the grid side converter; furthermore, no extra hardware is required. The feasibility of this design has been proven by means of mathematical model and digital simulations based on Matlab/Simulink.

1.4 Study Objectives

The first part of the study focuses on wireless health monitoring systems for the wind turbine system. Since the unforeseen failures of component—especially on the rotating parts in a wind turbine or generator—have a significant impact on the wind turbine economy, the best approach is to employ a wireless heath monitoring of electrical machine by applying vibration analysis to detect rotor imbalance conditions. The next part proposes a new control technique for the rotor side inverter controller that would guarantee the controllability of DFIG during the rotor imbalance condition without adding extra hardware. This would also improve the quality of wind turbine output during rotor imbalance conditions. This technique reduces the oscillation of wind turbine output by control from a rotor side inverter, which requires lower power injection compared with the grid side converter, with no extra hardware required.

1.5 Synopsis of Chapters

The organizational structure of this dissertation is as follows:

Chapter 1 introduces the general background of health monitoring system of wind turbines, wind turbine failures and fault detections, illustrating the importance, motivation and study objectives of this dissertation.

Chapter 2 reviews the historical research approaches and techniques, discussing the conventional and other methods used for fault diagnostic in detail.

Chapter 3 describes the proposed wireless electrical machine health monitoring system in detail. This chapter focuses mainly on condition based monitoring, vibration sensor equipment, and machine vibration analysis. The ZigBee based wireless network communication is also described. All design guidelines of hardware and software implementation are given.

Chapter 4 investigates the electrical machine under rotor imbalance conditions. The effect of machine vibration on vibration signature can be identified. The proposed rotor imbalance detection and severity level estimation is validated by hardware implementation. All details of experimental setup and results are also given.

Chapter 5 describes the overall control system of wind turbines. The wind turbine control level and the DFIG control level are illustrated. The conventional operation of the grid side converter and the rotor side inverter are presented. The aerodynamic model, gearbox and DFIG mathematical model are also included in this chapter. The disadvantages of the conventional rotor side inverter controller design are discussed.

Chapter 6 presents the overall control system of the proposed rotor side inverter controller. The stator flux magnitude and phase angle estimator is illustrated. The oscillating rotor current extraction and the stator current estimator are systematical designed. The conventional decoupling voltage control is modified to be able to perform better current control via a current-controlled voltage source PWM inverter which can suppress the oscillation of the

output of the wind turbine. The simulation results of four different events of real wind speed data from ERCOT system are given.

Chapter 7 states the summary and contributions of this dissertation and discusses the opportunities for further research.

CHAPTER 2

LITERATURE REVIEW

2.1 Present Wind Turbine Condition Monitoring and Fault Diagnosis

Wind turbine condition monitoring systems collect data from the main components of a wind turbine such as the generator, the gearbox, the main bearing, the shaft, and the yaw system. The purpose of this data-gathering is to minimize downtime and maintenance costs while increasing energy availability and the lifetime service of wind turbine components. An ideal condition monitoring system would monitor all the components using a minimum number of sensors.

There have been a few literature reviews on wind turbine condition monitoring. As renewable energies have gained dramatically increasing attention from industries and academia, a great deal of new research has been reported with regard to condition monitoring and fault diagnosis [11-19]. This chapter aims to review the most recent advances in condition monitoring and fault diagnostic techniques with a focus on wind turbines and their subsystems related to mechanical fault. This section summarizes the monitoring and diagnostic methods for the major subsystems in wind turbines such as gearbox, bearing, and generator which are the primary focus of this study.

2.1.1 Gearbox and Bearing

Gearbox fault is widely acknowledged as the leading issue for wind turbine drive train condition monitoring among all subsystems [11-19]. Gear tooth damage and bearing faults are both common in the wind turbine. According to McNiff [27], bearing failure is the leading factor in turbine gearbox problems. In particular, it was pointed out that the gearbox bearings tend to fail in different rates. Among all bearings in a planetary gearbox, the planet bearings, the intermediate shaft-locating bearings, and the high-speed locating bearings tend to fail at the

fastest rate, while the planet carrier bearings, hollow shaft bearings, and non-locating bearings are least likely to fail. This study indicates that more detailed stress analysis of the gearbox is needed in order to achieve a better understanding of the failure mechanism and load distribution which would lead to improvement of drive train design and sensor allocation.

Vibration measurement and spectrum analysis are typical choices for gearbox monitoring and diagnostics. For instance, Yang et al. developed a neural network based diagnostic framework for gearboxes in [28]. The relatively slow speed of the wind turbine sets a limitation in early fault diagnosis using the vibration monitoring method. Therefore, acoustic emission (AE) sensing, which detects the surface stress waves generated by the rubbing action of failed components, has recently been considered a suitable enhancement to the classic vibration based methods for multisensory monitoring scheme for gearbox diagnosis, especially for early detection of pitting, cracking, or other potential faults.

Lekou et al. presented their study using AE in parallel with vibration, temperature, and rotating speed data for health monitoring [29]. It was shown that monitored periodic statistics of AE data can be used as an indicator of damage presence and damage severity in wind turbines.

Chen et al. [30] set up a finite-element (FE) simulation study of stress wave based diagnosis for the rolling element bearing of the wind turbine gearbox. It is noteworthy that FE analysis is a good complementary tool to the experimental based study, with which the physical insight of various levels of faults can be investigated. Notice that AE measurement features very high frequencies compared to other methods, so the cost of data acquisition systems with high sampling rates needs to be considered. Besides, it is noise-rich information from AE measurement. Advanced algorithms are needed to extract useful information.

Yang et al. [17] presented a more comprehensive study on diagnosis for the drive train of wind turbines with synchronous generators. In particular, the discrete wavelet transform (DWT) was employed to deal with the noise-rich signals from wind turbine measurements. For

mechanical faults of the drive train, the electrical analysis was investigated. Diagnosis of gear eccentricity was studied using current and power signals. It is noteworthy that the data were obtained from a wind turbine emulator, incorporating the properties of both natural wind and the turbine rotor aerodynamic behavior. Although the level of turbulence simulated was not described, the demonstrated performance was still promising for practical applications.

Torque measurement has also been utilized for drive train fault detection. The rotor faults may cause either a torsional oscillation or a shift in the torque-speed ratio. Such information can be used to detect rotor faults, e.g. rotor mass imbalance [4]. Also, shaft torque has a potential to be used as an indicator for decoupling the fault-like perturbations due to higher load. However, inline torque sensors are usually expensive and difficult to install. Therefore, using torque measurement for drive train fault diagnosis and condition monitoring is still not practically feasible.

2.1.2 Generators

The wind turbine generators are also subject to failures in bearing, stator, and rotor among others components. For induction machines, about 40% of failures are related to bearings, 38% to the stator, and 10% to the rotor [31]. The major faults in induction machine stators and rotors include inter-turn faults in the opening or shorting of one or more circuits of a stator or rotor winding, abnormal connection of the stator winding, dynamic eccentricity, broken rotor bars of cracked end-rings for cage rotor, static and/or dynamic air-gap eccentricities, among others. Faults in induction machines may produce some of the following phenomena: unbalances and harmonics in the air-gap flux and phase currents, increased torque oscillation, decreased average torque, increased losses and reduction in efficiency, and excessive heating in the winding.

Popa et al. conducted an experimental study on fault diagnosis of doubly-fed induction generators (DFIG) [31]. Machine current signature analysis (MCSA) was investigated for turn-

to-turn faults based on generator current spectrum analysis. The stator and rotor currents as well as the power signals were used for diagnostics.

Watson and Xiang [32] used power signals to detect generator rotor misalignment and bearing faults using both fast Fourier transform (FFT) and wavelet analysis. Fast Fourier Transform analysis was used to determine the amplitude of the harmonic components more accurately, and thus to help find the peak amplitude spectrum of the wavelet coefficients during the given time period, which could be used as the fault signature. The results showed success in identifying the early stage of failures.

2.2 Review Conclusions

To achieve an accurate and reliable condition monitoring system for wind turbines, it is necessary to select measurable parameters as well as to choose suitable signal processing methods. In some examples, electrical sensors installed around the generator are highly recommended as they are non-invasive and easy to implement compared to the mechanical ones. In wind turbines, because of the noisy environment due to the presence of power electronics converters, signal to noise ratio of measured signals is low and the usage of electrical parameters are often more problematic than in a lab environment. Inaccurate signal analysis leads to various false alarms which makes fault detection unreliable.

To overcome this drawback, several approaches have been proposed by introducing the vibration measurement and using vibrations as an index for detecting mechanical fault in the system. However, those methods have been applied mostly for drive train failure, bearing faults, and gear tooth damage by using acoustic emission (AE) techniques for detection. Therefore, to enhance the effectiveness and thorough of condition-based predictive maintenance, dissertation proposes a vibration based monitoring system for rotor imbalance conditions.

CHAPTER 3

THE PROPOSED WIRELESS HEALTH MONITORING SYSTEM

The core objectives of this proposed wireless health monitoring system are to detect the present health condition of the machine, to prevent catastrophic failures caused by rotor imbalance, to improve the power quality before the problem is corrected, to predict the severity level of fault, and to estimate the useful life of the machine. The use of this type of health monitoring system helps to reduce the failure frequency and amount of downtime, maximize the utilization of the wind turbine, and minimize the maintenance overhead and cost due to production lost. Moreover, under the wireless sensor network system, there is no need to install wiring for data collecting and monitoring, thus eliminating the cost of installation and maintenance that would be required by communication cables.

3.1 Condition based Monitoring System for Wind Turbines

Condition based monitoring [6-9], which is generally referred to as a predictive or proactive maintenance, is a reliable and cost-effective approach in maintaining and running expensive equipment and machines. It is important to identify which technologies for monitoring machine condition will be the most useful and cost-effective in achieving goals and objectives. Each technique is limited to specific types of machinery and is useful in identifying specific types of faults. Each technique also provides different short-term and long-term economic benefits. A variety of technologies can be used as part of an advanced condition based monitoring system.

In this work, we mainly focus on the monitoring of wind turbines, as mechanical components or electrical machines account for the majority of wind turbine equipment, and vibration monitoring is thus a key component of this condition based monitoring system. It has been known for a long time that the integrity of the machine can be evaluated by detailed analysis of the vibration signals. The vibration signals carry information about structural

resonance and other components in the machine by means of vibration transducer. When the machine is in good condition and is running under normal operating conditions, it produces a certain vibration pattern specific to its vibration behavior and character, but as degradation starts in, the characteristics of the vibration signals changes.

However, vibration monitoring cannot provide all of the information that is required for a successful condition based monitoring system and is still limited to monitoring only the mechanical condition, not other parameters necessary for maintaining the reliability and performance of the equipment such as the severity level of abnormality or remaining usable life. Therefore, an advanced machine health condition monitoring system and fault prediction algorithms for particular rotor imbalance conditions are still needed today.

3.2 Vibration Sensor Equipment

In the wind power industry, vibration monitoring is used primarily to detect faults in mechanical components such as the bearings and gears installed inside the wind turbine nacelle. Figure 3.1 shows the major turbine components necessary for any wind turbine generator [32].

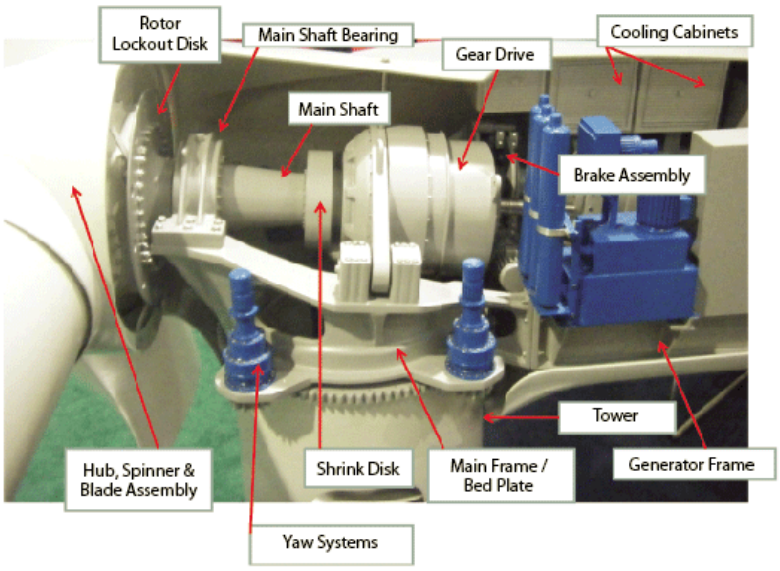

Figure 3.1 Major Components of Wind Turbine

The monitoring and fault prediction functions of a condition based monitoring system are based on robust sensor equipment for continuous measurements, and this system performs online evaluation of characteristic fault indicators by use of modern digital signal processing methods. Modern type wind turbines are mainly based on rotational components. Therefore, measurement of vibration on component housings and structural oscillation will yield data for calculating characteristic values by means of advanced condition monitoring and fault prediction algorithms.

The vibration signature from different kind of fault is unique and depends on the geometry, load, and speed of the components. Figure 3.2 shows a possible configuration of sensors installed on the drive train [32]. The type of sensor depends more or less on the frequency range relevant for the monitoring.

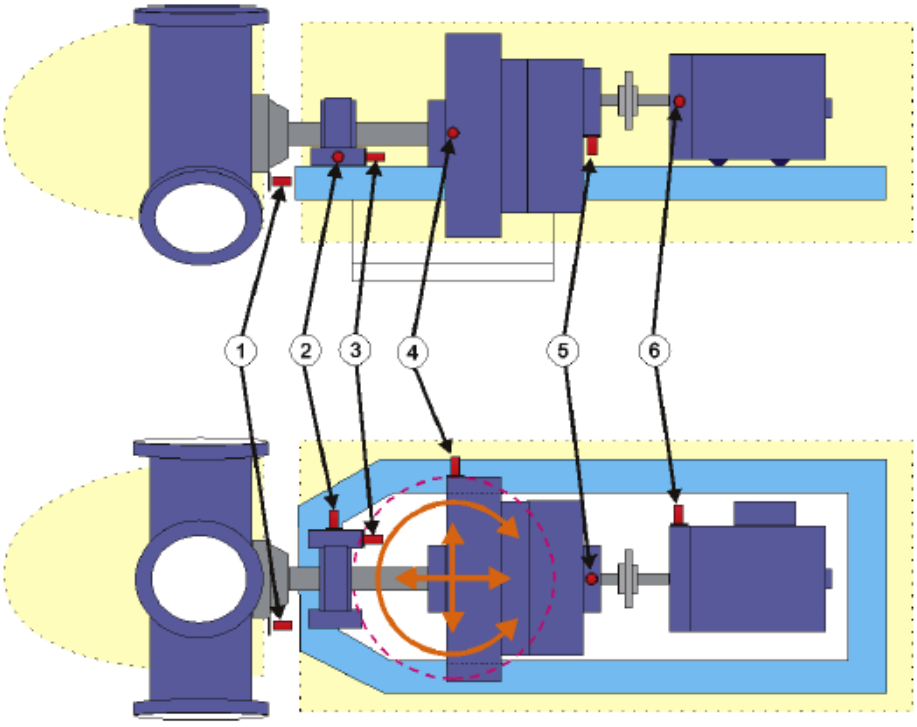

Figure 3.2 Common Sensor Configurations for Horizontal Axis Wind Turbine

The sensor configuration shown in Figure 3.2 allows nacelle oscillation measurement in both axial and transverse directions in relation to the rotor axis. By use of two transverse directed sensors in front of and behind the vertical tower axis, measurement of torsional oscillation of the nacelle can be performed.

These nacelle oscillations for wind turbine characteristic values used in fault detection are induced by rotating the low-speed shaft of the wind turbine. Therefore, they have to be measured at very low frequency. This measurement can be done with static accelerometers. This means that the sensor has a low cut-off frequency. Internally, the sensors measure the force applied to a probe mass, either by acceleration or by gravitational force. There are sensors available on the market that have integrated the complete electronics for strain gauge amplifiers and output signal converters. These sensors only need an external power supply to deliver voltage or current signals for an analog signal conditioning circuit. The mounting positions of the sensors are indicated with labels 2, 3 and 4. These positions allow the measurement of the nacelle oscillation modes.

For monitoring of the gearbox, bearing, and generator conditions, the vibration sensors operating at a frequency range from 1 Hz to 20,000 Hz will be used to measure the vibration induced by gearwheels, bearings, and rotating part of generators. Labels 5 and 6 show an example for the position of the gearbox and generator vibration sensors. For large wind turbines of multi-megawatt class, additional sensors can be mounted on the housings of gearbox and generator. These vibration sensors can be mounted with glued sockets on every plane surface of a gearbox or generator housing or on the supporting structure of the wind energy converter. The area needed is about 5 cm in square. Installation of these vibration sensors can easily be done even after the wind turbine system has been constructed.

3.3 Machine Vibration Analysis

Vibration analysis [33-35] is a proven and effective technology being used in condition monitoring. For the measurement of vibration, different vibration transducers are applied,

according to the frequency range. Vibration measurement is commonly done in the gearbox, turbines, bearings, and shaft. For wind turbine application, the measurement is usually done at critical locations where the load condition is at maximum, for example, wheels and bearings of the gearbox, the main shaft of turbine, and bearings of the generator. Different types of sensors are employed for the measurement of vibration: acceleration sensors, velocity sensors, and displacement sensors. Different vibration frequencies in a rotation machine are directly correlated to the structure, geometry, and speed of the machine. By determining the relation between types of defects and their characteristic frequencies, the causality of problems can be determined, and the remaining useful life of components can be estimated. The history of the equipment, its failure statistic, vibration trend, and degradation pattern are of vital importance in determining the health of the system and its future operating condition.

Using vibration analysis, the presence of a failure, or even an upcoming failure, can be detected because of the increase or modification in vibrations of industrial equipment. Since an analysis of vibrations is a powerful tool for the diagnosis of equipment, a number of different techniques have been developed. There are methods that only distinguish failures at a final state of evolution and there are others, more complex, that identify defects at an early phase of development. In general, there are two main approaches used for processing the signal: time domain and frequency domain. It is important to use the method that is best suited for each particular piece of equipment, and in this research both the time domain approach and the frequency domain approach will be employed to extract useful features of the signal and obtain information about the machine's behavior due to various operating conditions.

3.3.1 Time Domain Approach

Time domain signals of vibration level in the machine were used in the early stages of vibration analysis when primarily analog instruments were available and newer technologies (i.e. Fast Fourier Transform, microprocessors) were not available. A time domain vibration signature is also called time trace or time plot.

3.3.1.1. Implementation of Trend Monitoring

This technique acquires overall vibration readings from select points on the machine. These data are then compared with a baseline reading taken from a new machine to determine the relative condition of the machine. Normally this measurement provides total vibration energy between 10 and 10,000 Hz and therefore it is only providing information on the overall state of the component, not giving any information about failure modes. Specific machine problems and faults cannot be isolated and identified.

Moreover, another problem with Trend Monitoring is that wind turbines don't work at a constant speed or under constant operational conditions, which means that parameters have to be normalized with respect to the operational condition. To overcome this problem, machine manufacturers need to provide the correlation information of the rotor speed and output power of the turbine with the vibration measurements.

3.3.1.2. Implementation of Signal Averaging

Time domain averaging is effective in suppressing signals that are not correlated within the averaging period. Let the signal strength be denoted by S and let the standard deviation of a single measurement be σ. This represents the noise in one measurement N. If n measurements are added together, the sum of signal strengths will be nS. For the noise, the standard error propagation formula shows that the variance, σ^2, is additive. The variance of the sum is equal to $n\sigma^2$. Hence the signal-to-noise ratio, S/N, is given by

$$\frac{S}{N} = \frac{nS}{\sqrt{n\sigma^2}} = \sqrt{n}\frac{S}{\sigma} \tag{3.1}$$

Thus, in the ideal case S/N increases with the square root of the number of measurements that is averaged. In practice, the assumptions may be not fully realized, resulting in a lower S/N improvement than in the ideal case. To obtain better results, it is also necessary

to know the repetition frequency precisely and sampling the signal with an integer number of samples per period (x). Noise reduction goes as $\frac{1}{\sqrt{x}}$, greatly increasing the signal to noise ratio.

The underlying assumption is that the shaft rotation speed is constant. This approach assumes that the shaft speed is known with a good deal of precision. Some measurement error in the shaft speed serves to mistune the filter, giving poor results, an outcome that can always be expected. Hence, it is required that the data acquisition system should have adaptable sampling rate according to the current shaft speed of the machine. This requirement is difficult to meet in practice and some of these problems have been previously addressed as well. Therefore, using this approach in the vibration analysis has some serious drawbacks in machinery diagnostics.

3.3.1.3. Implementation of Root Mean Square

The RMS value of the vibration signal is used for primary investigation of the machine health. The RMS values will be used to detect the severity of the abnormal condition. These values could also be used as input to training the neural network based fault classifier.

For the case of a set of n values $\{x_1, x_2, ..., x_n\}$, the RMS value is given by

$$RMS = \sqrt{\frac{x_1^2 + x_2^2 + ...x_n^2}{n}} \tag{3.2}$$

3.3.1.4. Implementation of Crest factor

The crest factor is the ratio of the peak value of the vibration signal to the RMS value.

$$Crest\ factor = \frac{Peak\ Value}{RMS\ Value} \tag{3.3}$$

The purpose of the crest factor calculation is to give the analyst a quick idea of how much impacting is occurring in a waveform. It is meaningful where the peak values are reasonably uniform and repetitive from one cycle to another. Crest factor is often used to

indicate faults in the rolling element bearings. The rotor imbalance faults do not affect the value of crest factor. These values can give qualitative information about the machine condition if it is compared to the vibration signal standard and can be used to differentiate the bearing fault and rotor imbalance fault. The values of the crest factor of the vibration signal in the healthy case will be used as a baseline condition in health monitoring system. Continuous monitoring of crest factor along with the historical record can provide useful information about bearing condition. Using both the RMS value and the crest factor for the machine health diagnostic may increase the overall system performance for health monitoring systems.

3.3.2 Frequency Domain Approach

Fast Fourier Transform (FFT) is the most common way to transform signals in the frequency domain. The advantage of frequency domain analysis over time domain analysis is its ability to identify and isolate particular frequency components of interest. FFT is an algorithm that enables evaluation of the Fourier transform of a periodic signal through a signal processor. Frequency domain analysis is often applied in gearboxes and bearings because each component and its associated failure modes in rotating machinery are characterized by a determined frequency.

In most research, the frequency domain analysis is attractive because it provides more detailed information about the status of the machine, whereas the time domain analysis can give only qualitative information about the machine condition. In general, machine vibration signal is composed of three parts: stationary vibration, random vibration, and noise. Traditionally, Fourier transform (FT) was used to perform such analysis. If the level of vibrations and the noise are high, inaccurate information about the machine condition may be obtained.

3.3.2.1. Implementation of Spectrum Analysis

The Fast Fourier Transform (FFT) algorithm is used to extract some useful features of the vibration signal, and the set of frequency components related to different types of faults can thus be obtained. Basically, the computational problem for the discrete Fourier transform (DFT)

is to compute the sequence $\{X(k)\}$ of N complex-valued numbers given another sequence of data $\{x(n)\}$ of length N, according to the formula:

$$X(k) = \sum_{n=0}^{N-1} x(n) e^{-j2\pi \frac{kn}{N}}, \ 0 \le k \le N-1 \tag{3.4}$$

In order to achieve the earliest possible recognition of a fault in the machine, a comparison of the spectrum of the machine with the spectrum of the healthy case must be performed. The amplitudes of the frequency components can be used to specify the degree of fault for various operating conditions. From the literature it can be observed that the first rotational harmonic has a dominant value.

In the proposed work, the vibration signal information will be sampled and stored in the computer memory. Both the time domain and frequency domain approach will be used to obtain the machine's health condition. All the techniques mentioned here for signal analysis and processing will be implemented by MATLAB software. Based on the vibration spectrum analysis, it is normally straightforward to locate the mechanical rotational frequency by monitoring the vibration spectrum and finding the most significant peak in the expected rotational frequency range. This peak amplitude at the rotational frequency serves as the rotor imbalance indicator for the proposed monitoring system. Furthermore, the amplitude of this frequency component reveals the severity level of the rotor imbalance fault. A block diagram of the proposed severity detection of rotor imbalance is shown in Figure 3.3.

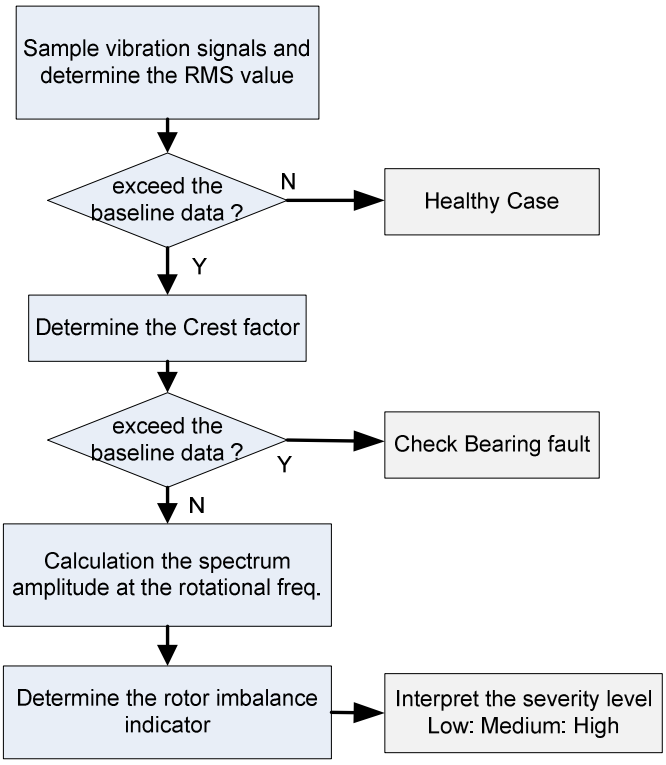

Figure 3.3 Block Diagram of the Proposed Severity Detection Technique of Rotor Imbalance

3.4 Wireless Network Communication

3.4.1 ZigBee/IEEE 802.15.4 Standard

The IEEE 802.15.4 standard [36] defines the protocol and interconnection of devices via radio communication in a personal area network (PAN). It operates in the ISM (Industrial, Science and Medical) radio bands, at 868 MHz in Europe, 915 MHz in the USA and 2.4 GHz worldwide. The purpose is to provide a standard for ultra-low complexity, ultra-low cost, ultra-low power consumption and low data rate wireless connectivity among inexpensive devices. ZigBee technology may be used in various applications in industrial controls, embedded sensors, medical devices, smoke and intruder alarms, building and home automation and others. The network is designed to use very small amounts of power, so that individual devices might run for one year or more with a single alkaline battery. Based on these features, the ZigBee technology is very suitable for this application. The ZigBee network layer supports star,

tree and mesh topologies. In a star topology, the network is controlled by a single device called the ZigBee coordinator (as master node). The ZigBee coordinator is responsible for initiating and maintaining the devices within the same network, and all other devices known as end devices (slave nodes), directly communicate with the ZigBee coordinator.

There are two types of devices in an IEEE 802.15.4 wireless network: full-function devices (FFDs) and reduced-function devices (RFDs). An FFD is capable of performing all the duties described in IEEE 802.15.4 standard and can accept any role in the network. An RFD, on the other hand, has limited capabilities. RFD devices are intended for very simple applications such as turning on or off the switch. The processing power and memory size of RFD devices are normally less than those of FFD devices. In ZigBee standard terminology, a ZigBee coordinator is an IEEE 802.15.4 PAN coordinator. The ZigBee coordinator is responsible for initiating and maintaining the devices within the same network. A ZigBee router is a device that can act as an IEEE 802.15.4 coordinator. Finally, a ZigBee end device is a device that is neither a coordinator nor a router (slave nodes), but directly communicates with the ZigBee coordinator.

3.4.2 ZigBee based System Framework

The system framework for a health monitoring system based on a wireless sensor network is shown in Figure 3.4. It is made up of data collection nodes and a PAN network coordinator. The data collection nodes on this proposed system include an accelerometer. Network node can be set up in several nearby collection points. The nodes can carry out desired functions such as detecting the current/vibration signals, signal quantizing, simple processing, and the ZigBee™/IEEE802.15.4 Standard package framing to transmit data to the PAN network coordinator. In addition, they can also receive data frames from other nodes, and then, adding multi-hop information, package framing, and then transmit the new data frames to the network coordination in the same manner. Upon receiving that data via the PAN network coordinator, the base station will upload the incoming data to computer for further processing and analysis.

An advanced diagnostic/prognostic algorithm will be used to analyze the data to determine the health status of the machine and suggest possible measures to mitigate potential issues. The data can also be transmitted through the Internet for remote fault diagnosis.

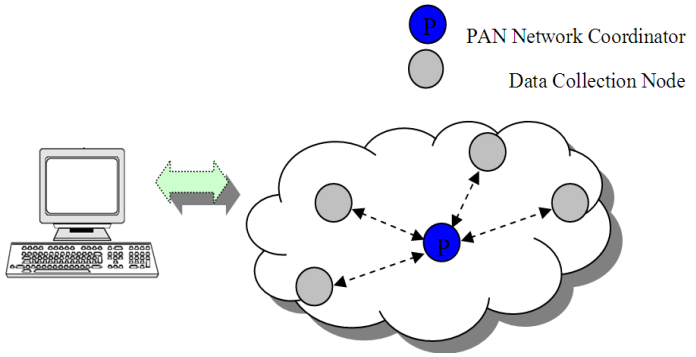

Figure 3.4 Structure of the Wireless Sensor Network

3.4.3 Hardware Design of Node and Base Station

The hardware framework is illustrated in Figure 3.5. It is comprised of node and a base station. The main circuits include the power supply circuit, CC2430 System on chip and external circuit [37], sensor and signal conditioning circuits, flash ROM and RAM memory, serial port interface, and three LEDs for status indication.

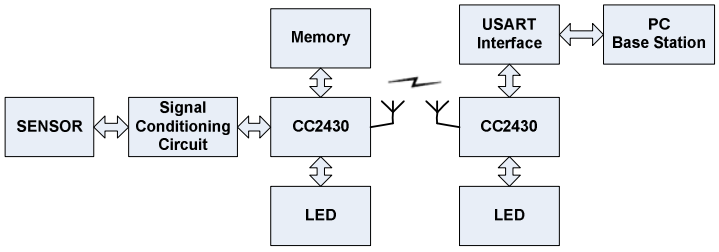

Figure 3.5 Hardware Framework

3.4.3.1. CC2430 Introduction

In this proposed system design, we adopt the IEEE 802.15.4 standard compliant transceiver CC2430 from Texas Instruments. The CC2430 is a true System-On-Chip for wireless sensor networking ZigBee™/IEEE802.15.4 solutions for a 2.4GHz wireless sensor network. It combines the excellent performance of the leading CC2420 RF transceiver with an

industry-standard enhanced 8051 microcontroller (MCU), with 128 KB flash memory and 8 KB RAM. Both the embedded 8051 MCU and the radio components have very low power consumption. The CC2430 also includes 12-bit ADC (Analog-to-Digital Converter) with up to eight inputs and configurable resolution. Combined with the ZigBee protocol stack (Z-Stack) from TI, the CC2430 is one of the most competitive ZigBee solutions in the industry.

3.4.3.2. ADXL330 MEMS Accelerometer

The ADXL330 [38] is a complete three-axis acceleration measurement system on a single monolithic IC. The ADXL330 has a measurement range of ±3 g. The block diagram is illustrated in Figure 3.6. It contains a micro-machined sensor and signal conditioning circuit to implement the open loop acceleration measurement architecture. The output signals are analog voltages that are proportional to acceleration. The accelerometer can measure the static acceleration of gravity in tilt sensing applications as well as dynamic acceleration resulting from motion, shock, or vibration. Deflection of the structure is measured using a differential capacitor that consists of independent fixed plates and plates attached to the moving mass. The fixed plates are driven by 180° out-of-phase square waves . Acceleration deflects the moving mass and unbalances the differential capacitor resulting in a sensor output whose amplitude is proportional to acceleration. Phase-sensitive demodulation techniques are then used to determine the magnitude and direction of the acceleration.

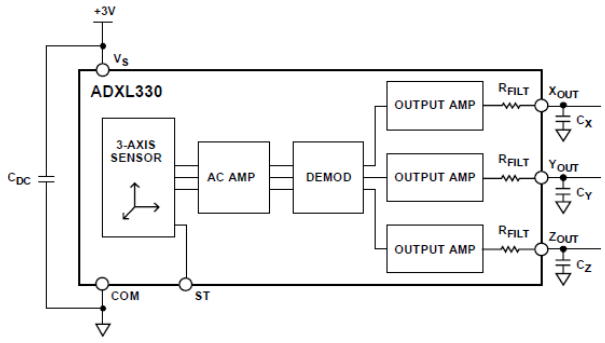

Figure 3.6 Block Diagram of ADXL330 MEMS Accelerometer [38]

The demodulator output is amplified and brought off-chip through a 32 kΩ resistor. The user then sets the signal bandwidth of the device by adding a capacitor. This filtering improves measurement resolution and helps prevent aliasing. The user selects the bandwidth of the accelerometer using the CX, CY, and CZ capacitors at the XOUT, YOUT, and ZOUT pins. Bandwidths can be selected to suit the application, with a range of 0.5 Hz to 1600 Hz for X and Y axes, and a range of 0.5 Hz to 550 Hz for the Z axis.

3.4.3.3. Node

The sensor nodes are in charge of collecting information such as current and vibration signal. Commonly, the original current signal amplitude and its ratio of signal to noise do not satisfy the A/D conversion circuit on the CC2430. Therefore, before being sent into ADC, the current signals are filtered and amplified as presented in the signal conditioning circuit. The ADC module of CC2430 has eight analog input pins which can be configured into eight single-ended inputs or four differential inputs. The current signals are digitized through a 12-bit analog to digital conversion at up to 2000 samples per second (2kHz). The storage unit has 128kb flash memory and 8kb RAM to be chosen. Controlled by the MCU, the data from the ADC can be temporarily stored in the storage unit 8kB RAM and then transmitted to the network coordinator node through the ZigBee module.

3.4.3.4. Base Station

The base station includes the network coordination and a personal computer. The network coordination is primarily responsible for distributing the network address to new rode, notarizing the physical address, and transmitting test data. The network coordination can connect and send the data and information to PC through RS232 or USB port.

3.4.4 Software Design

The IEEE 802.15.4 frame structure of the ZigBee protocol [39] is made up of data model, destination address, data length, data information, and checkout; the frame format is

shown in Figure 3.7. The first byte is a length byte. The length byte itself is not counted in the length. The frame control field is set according to the IEEE Std. 802.15.4-2006.

Octets: 1	2	1	2	2	2	5	Variable	2
Length Byte	Frame Control	Sequence number	Dest. PAN ID	Dest. Address	Source Address	Aux.Sec. Header	Frame payload	FCS

Figure 3.7 The Frame Format

The sequence number is an 8-bit value starting on 0 for the first packet transmitted after initialization. The values of the destination PAN ID, destination address and source address fields are configured by the application as part of the basic RF initialization.

The auxiliary security header is only included in the frames when the security features are used, for example when the compile option SECURITY_CCM is set in the project file. This field is 5 bytes long and consists of a security control byte that defines the level of protection applied to this frame, and frame counter.

The frame counter field of the auxiliary security header is 4 bytes long and is used for replay protection of the frame. The value of the frame counter field is set to 0 on initialization and incremented for each transmitted packet.

The frame payload is variable in length and consists of data sent from the above layer. The maximum length of this field is 103 Bytes. The Frame Check Sequence field (FCS) is 2 bytes long. This field is automatically appended by the radio chip. When a frame is received the first byte of FCS is replaced with the value in the RX FIFO on the radio.

3.4.5 Software Flow

The software flowchart mainly describes the working process of the network coordinator and data collection node. They are shown in Figure 3.8. The debugging and programming can be done directly in the Integrated Development Environment IAR Embedded Workbench for 8051 [40].

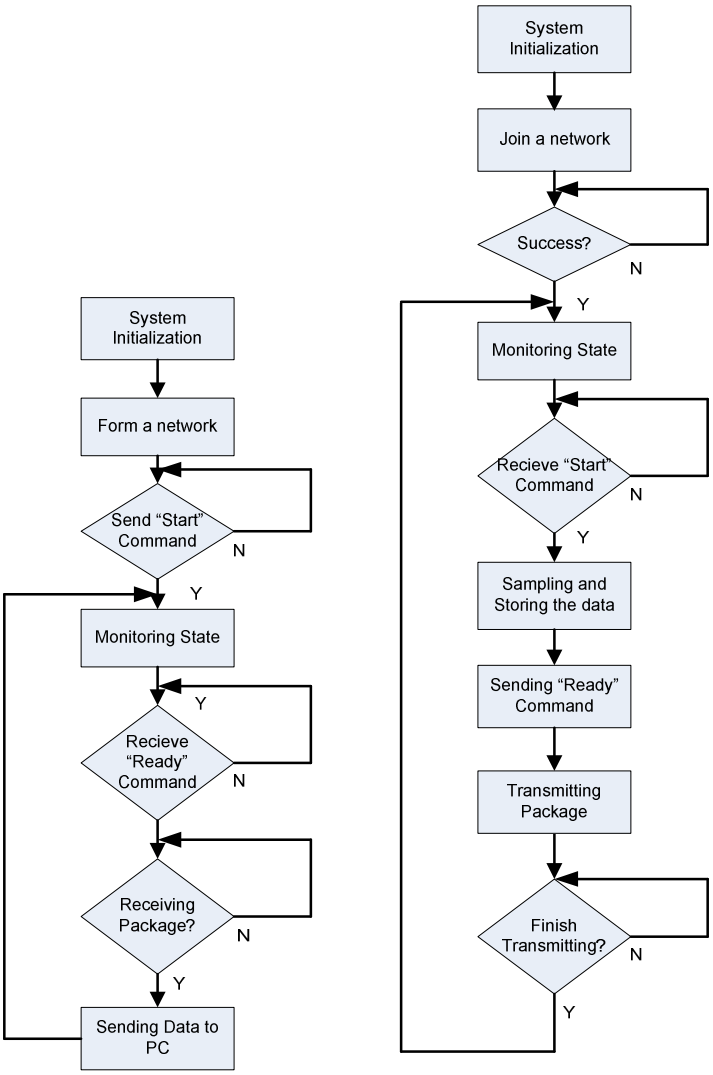

Figure 3.8 The Flow Chart of PAN Network Coordinator (left side) and Data Collection Node (right side)

As network coordinator, the CC2430 is initialized first, and then the protocol stack is initialized. The program will begin forming the network and allow the nodes to join the network. If the network is formed successfully, the network coordination will be waiting for user interrupt to send the "START" command to the node. If a node is ready to transmit the data, it will send the "READY" command to the network coordinator. Then the network coordinator will turn on the Radio frequency channel to prepare for the incoming package. Once all packages are received, it will send the data to PC via USB port.

As a data collection node, the program also initializes CC2430 and protocol stack first. Then it will start to join the network. If it can join the network successfully, it will be put into monitoring state to monitor whether there are any commands coming from the network coordinator. If a data collection node receives the “START” command, then it will perform the predefined task. After the end of ADC conversion, the node will store all of the sampling data in RAM and then send a command back to the network coordinator. After the node finishes transmitting all data, it will be returned back to monitoring state again.

CHAPTER 4

FAULT DETECTION OF INDUCTION MACHINE UNDER ROTOR IMBALANCE CONDITIONS

Rotor imbalances are common mechanical faults in electrical machines. In general, a mechanical fault in the load part of the overall system can be observed from the variation of the load torque. When a mechanical fault happens, it will result in a rotating eccentricity at the rotating frequency [41]. These faults may also cause speed oscillations that have an effect on the stator current and finally lead to additional undesired harmonic components of power and torque at particular frequencies in the spectra.

4.1 Induction Motor under Rotor Imbalance

To analyze the mechanical phenomena of the induction motor under rotor imbalance conditions, the dynamic nature of a mechanical system can be modeled as shown in Figure. 4.1

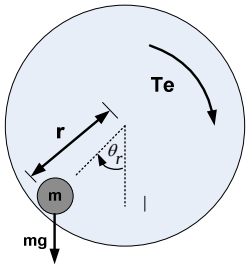

Figure 4.1 Rotational Model of Horizontally Mounted Mechanical System under Rotor Imbalance

Under the assumption that the mechanical system with the unbalance is horizontally installed along its rotational axis, the rotational dynamic for the torque equation is derived from the free body diagram as in Figure. 4.1. Rotor imbalance can be expressed by a mass of the total unbalanced weight (m) which is the main cause of the mechanical failure at the different speeds. This small mass is fixed on a disk mounted on the motor shaft. The different distances from the center of the rotating part (r) can be chosen. The gravity force (g) by the unbalanced mass produces the sinusoidal oscillating torque which is the function of the rotational frequency

(f_r) and the acceleration of gravity at the distance. The electromagnetic torque is produced by an induction machine and the rotational friction term is determined by the viscous damping constant and mechanical rotor speed that can be represented with the following equation:

$$J\frac{d^2\theta_r}{dt}+b\frac{d\theta_r}{dt}=T_e-mrg\sin(2\pi f_r t) \tag{4.1}$$

One can see that the torque equation is a function of time which comprises the constant component torque (T_e) and the additional component varying at the rotational frequency. It can be concluded that the rotor imbalance fault leads generally to periodic load torque oscillations. The influence of this torque oscillation on the induction motor results in a sinusoidal phase modulation of stator current which is equivalent to time-varying frequency and also leads to additional frequencies in the spectrum. Therefore, the total electromagnetic torque that is produced by the unbalanced load makes it possible to detect the rotor imbalance condition in an induction machine.

4.2 Effect on Vibration Signature

In general, there are various external sources of vibration with particular frequencies in rotating machinery. Other vibrations occur due to rotating asymmetries, such as rotor imbalance or misalignment. Among them, the largest low order vibration harmonic is normally due to the rotor imbalance of the rotational parts. From the vibration spectrum analysis, the low order harmonics are associated with the rotational frequency and can be distinguished from the lower range of the spectrum. The mechanical vibration due to rotor imbalance is a once per revolution force (at rotational frequency). Moreover, induction motors also vibrate at two times of the supply frequency due to the magnetic force between rotor and stator. This attraction force acts on the stator and induces the vibration on the motor frame. This also leads to a significant harmonic peak at twice the supply frequency in the vibration spectrum. Therefore, the harmonics of rotor imbalance can be modeled as an integer multiple of rotating frequency [41]:

$$f_{vib} = k.\left[f_s(\frac{1-s}{p}) \right] \quad (4.2)$$

Where f_s is stator supply frequency, k is the integer number, p is the number of pole pair, and s is the slip.

Based on the vibration spectrum analysis and for the sake of clarity, the higher order term are neglected in the following study since they have less influence in the spectrum than the fundamental term where $k = 1$. Hence, it is normally straightforward to locate the mechanical rotational frequency by monitoring the vibration spectrum and finding the most significant peak in the expected rotational frequency range.

4.3 Validation of Rotor Imbalance Detection

4.3.1 The Proposed Wireless Machine Health Monitoring System

The proposed wireless health monitoring system is shown in Figure 4.2. It comprises PWM inverter, induction motor and load station. The three-axis accelerometer mounted on the motor housing is used to measure the vibration of the motor. In this proposed wireless sensor system, the vibration signal from the three-axis accelerometer is recorded and stored at the base station. The recorded data are fed to monitoring system to evaluate the machine condition. Signal analysis is used to extract detailed information for an induction machine health diagnostic.

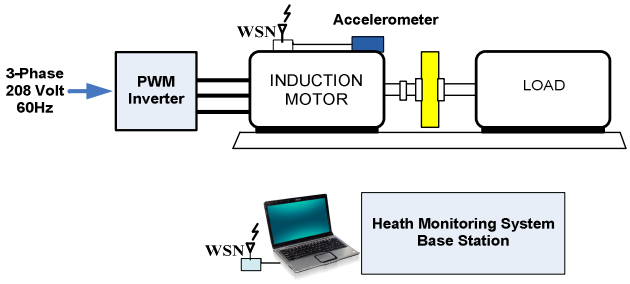

Figure 4.2 Schematic Diagram of the Wireless Machine Health Monitoring System

4.3.2 Experimental Setup

In order to validate the proposed vibration based health monitoring system, the test-bed for a mechanical fault was set up. Rotor imbalance was created on a 3-phase, 2-pole, 1 h.p.

squirrel cage induction motor. The induction motor is fed from the variable speed drive at 50Hz. The wireless sensor network is implemented and an accelerometer is also integrated in this monitoring system for detecting the vibration signals. Vibration signals were collected using ADXL330 tri-axial accelerometer mounted on the motor housing in Figure 4.3. The further machine vibration analysis is done by using Matlab software.

Figure 4.3 ADXL330 Tri-axial Accelerometer Mounted on the Motor Housing

The most important element of this test-bed is the flywheel (as shown in Figure 4.4) which has holes drilled in it. The weights applied to these holes produce an imbalance in the flywheel, and thus in the motor. The severity of the fault is determined by the weight. Axes of acceleration sensitivity corresponding to machine vibration are shown as in Figure 4.4.

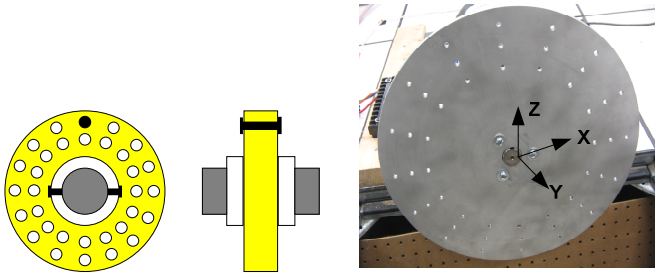

Figure 4.4 Flywheel Design used in Rotor Imbalance Test

Under the ZigBee wireless sensor network, all three-axis vibration signals are acquired at a sampling rate of 2kHz by a 12-bit ADC conversion. This can be done by data collection nodes, and all data is then transferred for further analysis at the base station by the PAN

network coordinator. The hardware development of the data collection node board and the network coordinator board in this study are shown in Figure 4.5.

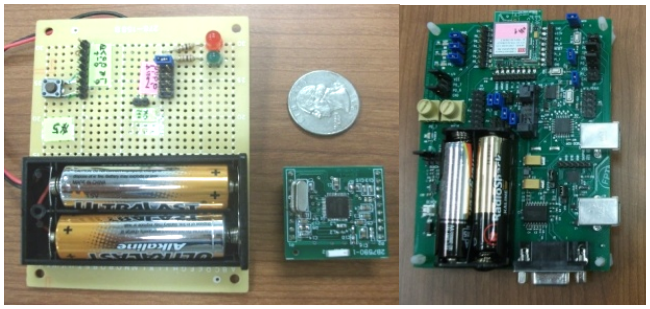

Figure 4.5 Example of a Data Collection Node Board (left side) and a PAN Network Coordinator (right side) Developed in this Study

4.3.3 Experimental Results

In order to examine how the vibration signals affect the detection of mechanical conditions, rotor imbalance conditions were induced mechanically to different degrees of intensity and the vibration on the machine frame was measured. Rotor imbalance was created using four different weights, namely, 5g, 10g, 15g and 20g. No-fault data was also collected to establish a baseline, considered as 0 g. All 3-axis vibration data were calculated as RMS values.

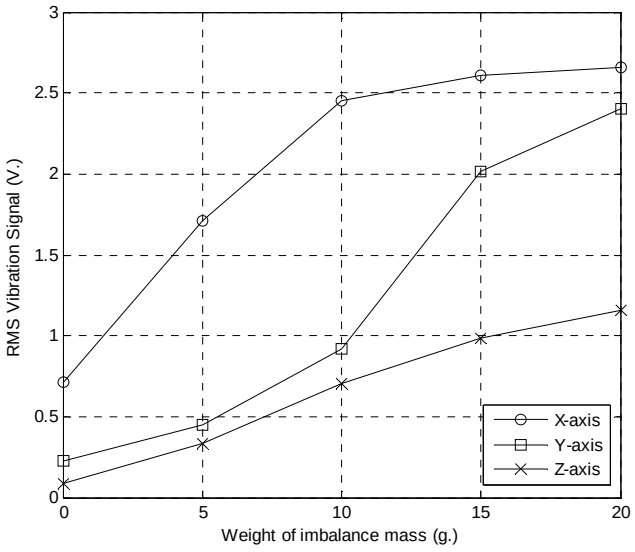

Figure 4.6 RMS Value of Vibration Signals from Different Imbalance Mass Tests

As shown in Figure 4.6, the RMS values increase corresponding to the weight of the imbalance mass. However, the change in crest factor is small as shown in Table 4.1. This implies that the degree of impact is relatively small from bearing faults.

Table 4.1 Crest Factor of Three-axis Vibration Signals from Different Imbalance Mass Tests

Imbalance Mass (g.)	Crest factor		
	X-axis	Y-axis	Z-axis
0 g.	1.457313235	1.7216206	2.18396705
5 g.	1.451261113	1.77381552	1.82287472
10 g.	1.387397149	1.50183948	1.63720601
15 g.	1.303934686	1.40032313	1.40077586
20 g.	1.249204942	1.45098092	1.29577839

In order to observe the frequency component amplitude of vibration signals related to rotor imbalance fault, the FFT algorithm is used to analyze the vibration signal. The three-axis vibration spectrum component amplitude at rotating frequency (50 Hz) is shown in Figure 4.7 and the amplitude of vibration spectra versus the different weights of imbalance mass are presented in Figure 4.8.

It can be observed that the rotational harmonic at 50 Hz has a dominant value. In addition, by increasing the weight of imbalance mass, the amplitude of this frequency component will increase in the spectrum. Therefore, the spectrum amplitude can be used to specify the degree of fault under known operating conditions.

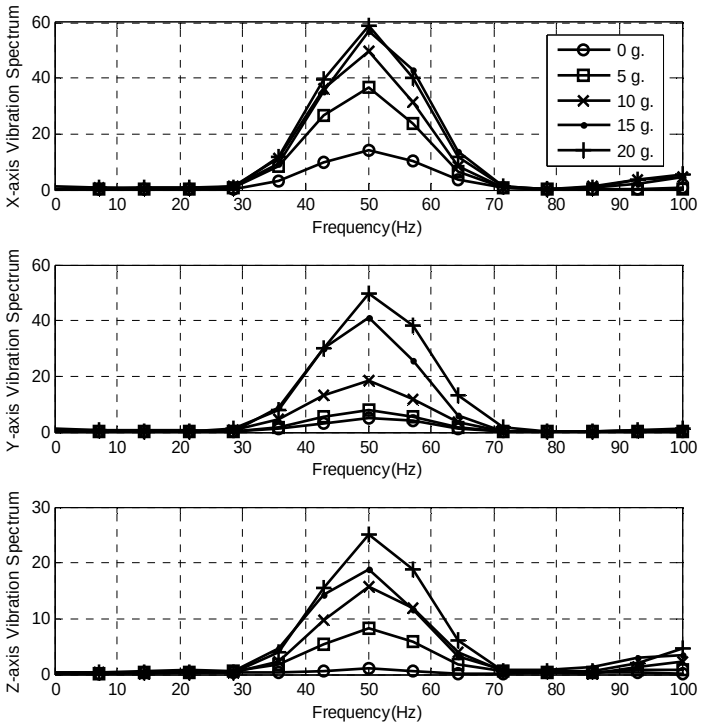

Figure 4.7 Three-axis Vibration Spectrum Component Amplitude at Rotating Frequency from Different Weights of Imbalance Mass

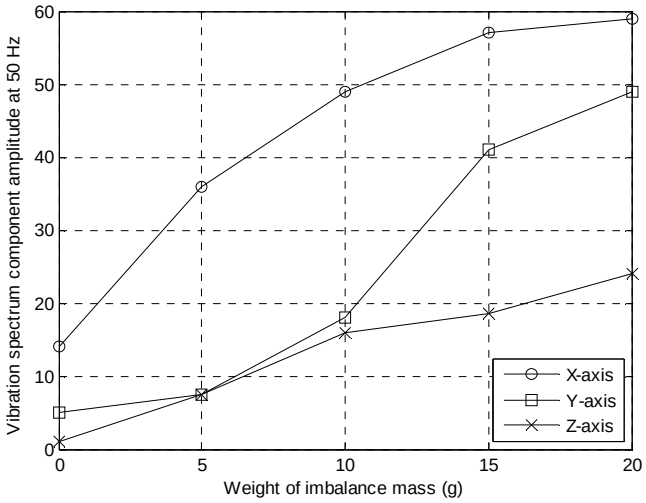

Figure 4.8 Three-axis Magnitude of Vibration Spectra at Rotating Frequency Versus the Different Weights of Imbalance Mass

Furthermore, based on the analyzed vibration data and the linear approximation, the relationship between the rotor imbalance indicator and the severity level can be represented in Figure 4.9. It is important to note that any estimation is subject to error. However, this relationship can be used as a trend to determine the severity level of the fault. For example, the change of rotor imbalance indicator during the time interval T0-T1 can be used to predict the change of the severity level. The result from the prediction will be a very useful part of the condition monitoring system and the estimation on the usable life of the equipment.

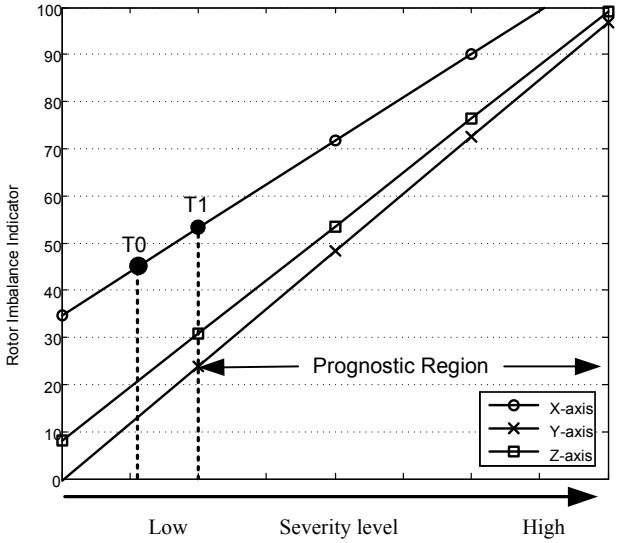

Figure 4.9 Rotor Imbalance Indicator of Different Levels of Imbalance Severity

4.4 Summary

The hardware and software design of a wireless health monitoring system for induction machine is presented. Vibration signals have been analyzed to detect the rotor imbalance condition. The implementations in time and frequency domain are given. The proposed rotor imbalance detection technique is verified with different level of severity. Rotor imbalance indicator can be used to estimate the range of severity level which is very useful part of the predictive maintenance. The wireless health monitoring system based on ZigBee wireless sensor network is tested under various operating conditions and is found to work satisfactorily.

CHAPTER 5

OPERATION OF WIND TURBINE SYSTEMS

The wind energy industry has developed rapidly through the last 10-20 years. Factories have gone from small-scale operations to a mature industry, and from a technical standpoint, wind turbines have increased in size, reduced in cost, and improved in the controllability. This makes modern wind energy a serious and competitive alternative to other energy sources.

The development has been concentrated on wind turbine systems for electrical power production, i.e. grid-connected wind turbines. Grid-connected wind turbines are a part of a power system with which they interact. The power system and its quality have an influence on the wind turbines' performance, lifetime, and safety. Therefore, the integration of wind power into the power systems has become an important issue in development and research of wind power [42-43].

The intention on this part of the proposed research focuses on studying, developing, and simulating wind turbine converter controllers, which mainly aim at improving the DFIG output under rotor fault conditions. The overall control system of a DFIG wind turbine will be examined first. It comprises the wind turbine control level and the DFIG control level. All important subsystems such as the aerodynamic model and the transmission model will also be illustrated. The conventional grid side converter and rotor side inverter are also included. Then we will discuss the performance of rotor side converter controllers with the focus on the disadvantages of current approach. An improved rotor side inverter controller is then proposed to make it possible to suppress the vibration during the occurrence of rotor imbalance conditions.

5.1 Overall Control System of DFIG Wind Turbines

A doubly-fed induction generator (DFIG) with a wound rotor induction generator and an AC/DC/AC IGBT-based PWM converter is commonly used in wind turbines. The stator is connected to the grid directly, whereas the rotor is fed at variable frequency through the AC/DC/AC converter. By using DFIG technology, maximum energy can be extracted from the wind when the speed is low by optimizing the turbine speed, and when the wind is strong, by reducing the mechanical stresses on the turbine.

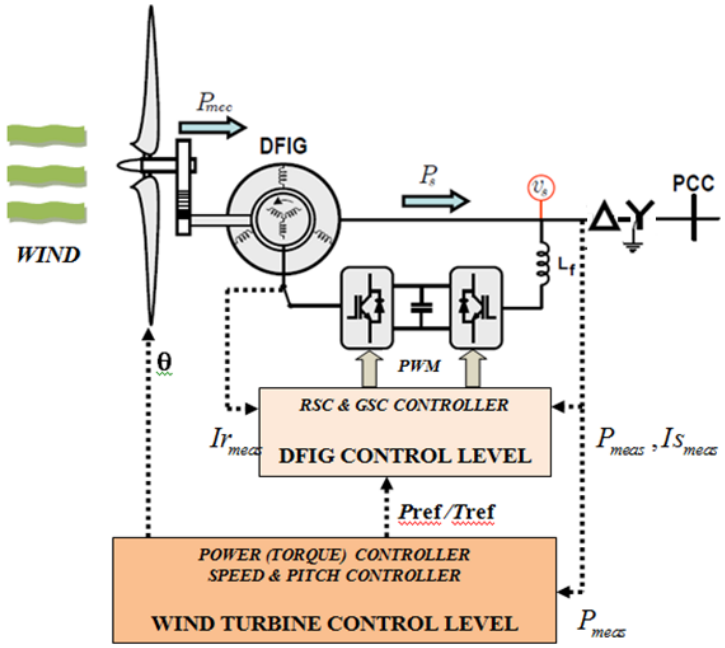

Figure 5.1 Wind Turbine Control System

As shown in Figure 5.1, the stator of the DFIG is connected directly to the incoming AC mains, whereas the wound rotor is fed from the power electronics converter through slip rings. This is to enable the DFIG to operate at different speeds, as wind speeds are changing from time to time. The DC link capacitor that connects the stator and rotor side inverters stores the power obtained from the induction generator for further generation usage. In this study, the overall control structure of the wind turbine system consists of an aerodynamic model, a

transmission system, a generator model, a DFIG control level block model, and a wind turbine control level block model [44].

5.2 Aerodynamic Model

The aerodynamic model is based on aerodynamic power efficiency, which depends on the pitch angle (θ) and on the tip speed ratio (λ). The function of the aerodynamic model is to compute the wind turbine mechanical power extracted from different wind speeds.

$$P_{rot} = T_{rot}.\omega_{rot} = \frac{\rho}{2} A_{rot} v_{wind}^3 C_p(\lambda, \theta) \tag{5.1}$$

5.3 Transmission System

In the transmission model, the emphasis is put only on those parts of the dynamic structure of the wind turbine that contribute to the interaction with the grid. Therefore, only the drive train is considered because this part of the wind turbine has the most significant influence on the power fluctuations.

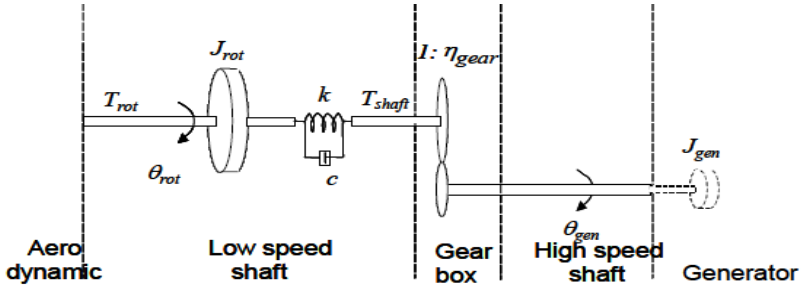

Figure 5.2 A Two-Mass Model

The transmission model is shown in Figure 5.2. It is essentially a two-mass model connected by a flexible low-speed shaft characterized by stiffness (k) and a damping (c). The high-speed shaft is assumed stiff. Moreover, an ideal gear with the exchange ratio $1:\eta_{gear}$ is included. The two masses correspond to the large turbine rotor inertia (J_{rot}) representing the blades and hub, and to the small inertia (J_{gen}) representing the induction generator.

5.4 Doubly Fed Induction Generator Model

Using Park's transformation from stationary (a-b-c) reference frame to rotating (d-q) reference frame, the dynamic model for a wound rotor induction machine (DFIG) is defined as follows [45]:

Stator voltage equations:

$$\begin{aligned} V_{sd} &= p\lambda_{sd} - \omega\lambda_{sq} + R_s i_{sd} \\ V_{sq} &= p\lambda_{sq} + \omega\lambda_{sq} + R_s i_{sq} \end{aligned} \tag{5.2}$$

Rotor voltage equations:

$$\begin{aligned} V_{rd} &= p\lambda_{rd} - (\omega - \omega_r)\lambda_{rq} + R_r i_{rd} \\ V_{rq} &= p\lambda_{rq} + (\omega - \omega_r)\lambda_{rd} + R_r i_{rq} \end{aligned} \tag{5.3}$$

Stator flux equations:

$$\begin{aligned} \lambda_{sd} &= (L_{ls} + L_m) i_{sd} + L_m i_{rd} \\ \lambda_{sq} &= (L_{ls} + L_m) i_{sq} + L_m i_{rq} \end{aligned} \tag{5.4}$$

Rotor flux equations:

$$\begin{aligned} \lambda_{rd} &= (L_{lr} + L_m) i_{rd} + L_m i_{sd} \\ \lambda_{rq} &= (L_{lr} + L_m) i_{rq} + L_m i_{sq} \end{aligned} \tag{5.5}$$

The electromagnetic torque, the power and reactive power equations may be written as:

$$\begin{aligned} T_s &= -\frac{3}{2} p(\lambda_{sd} i_{sq} - \lambda_{sq} i_{sd}) \\ P_s &= \frac{3}{2}(V_{sd} i_{sd} + V_{sq} i_{sq}) \\ Q_s &= \frac{3}{2}(V_{sq} i_{sd} + V_{sd} i_{sd}) \end{aligned} \tag{5.6}$$

The system dynamics, neglecting the friction loss, is given by:

$$J\frac{dw_r}{dt} = T_m - T_{em} \tag{5.7}$$

5.5 Wind Turbine Control Level Model

With slow dynamic response, this control level provides reference signals both to the pitch system of the wind turbine and to the DFIG control level. It contains two controllers: Power Controller and Pitch Controller.

5.5.1. Power Controller

This controller generates the active power reference signal for the active power control loop, performed by the rotor side inverter controller in the DFIG control level. In order to obtain the maximum power point tracking, this reference signal is determined from the predefined characteristic power-speed look-up table, illustrated in Figure 5.3, based on filtered measured generator speed. It is based on aerodynamic data of the wind turbine's rotor, and its points correspond to the maximum aerodynamic efficiency [46].

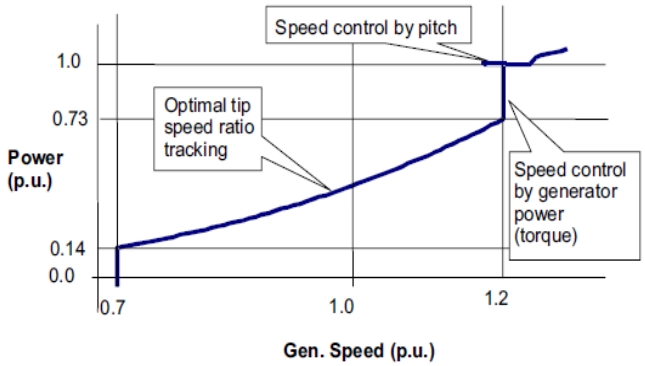

Figure 5.3 Power-Speed Tracking Characteristic

General Electric wind turbine 1.5-77 series model is adopted in this study as the tested wind turbine. All parameters of this series are shown in Figure 5.4, and the power-speed curve is presented in Figure 5.5.

1.5 MW Wind Turbine Series Models

	1.6–82.5	1.5–77
Rotor Diameter (m)	82.5	77
Hub Heights (m)	80/100	65/80
Frequency (Hz)	50/60	50/60
Vavg (m/s)	8.5	10.0
Vref (m/s)	40.0	45.0
Ve50 (m/s)	56.0	70.0
Cut-In (m/s)	3.5	3.5
Cut-Out (m/s)	25	25
IEC Wind Class	IEC TC IIB	IEC TC IB

Figure 5.4 General Electric's Wind Turbine 1.5-77 Series Model [46]

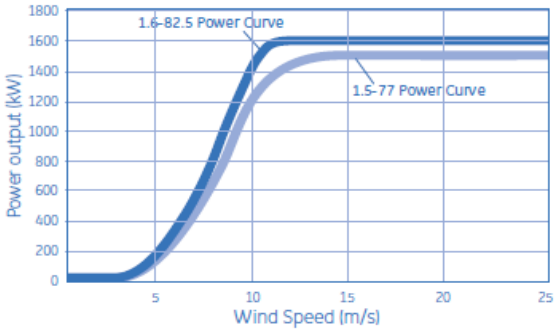

Figure 5.5 Power-Speed Characteristic of GE' Wind Turbine 1.5-77 Series Model [46]

5.5.2. Speed and Pitch Controller

The speed is controlled in order to follow the tracking characteristic. The error between the filtered measured generator speed and the rated generator speed is thus sent to the PI speed controller. The output of this PI controller is used as the reference pitch signal for the pitch system. In order to get a realistic response in the pitch angle control system, the servomechanism model accounts for a servo time constant τ_{servo} and the limitation of both the pitch angle (0 to 30 deg) and its gradient (±10 deg/s). Pitch compensation is implemented in order to compensate for the existing non-linear aerodynamic characteristics. The model of wind turbine control level is illustrated in Figure 5.6.

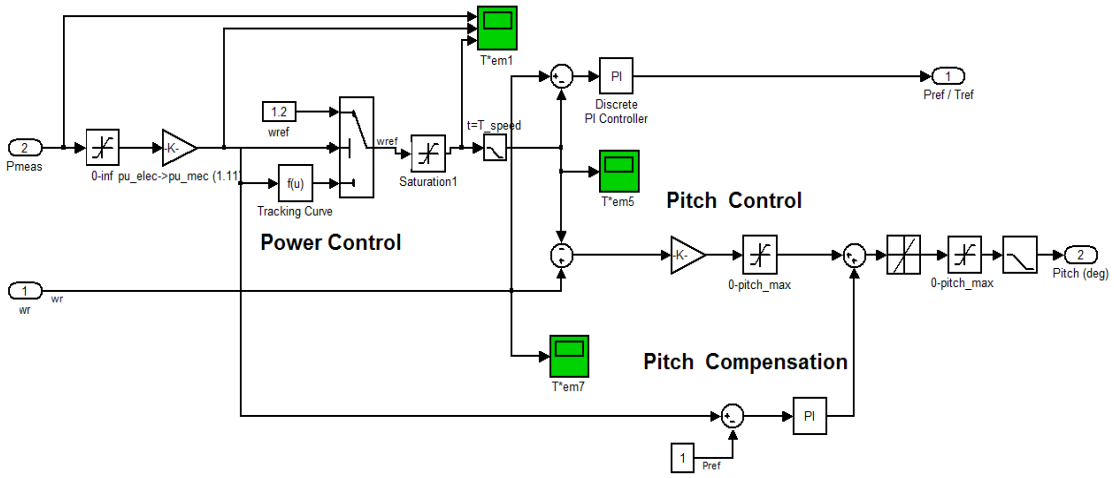

Figure 5.6 Wind Turbine Control Level

5.6 DFIG Control Level Model

With a fast dynamic response, this control level contains the electrical control of the power converters and of the doubly-fed induction generator. The DFIG control contains two controllers: Grid side converter controller and Rotor side inverter controller.

5.6.1. Grid Side Converter

The grid side converter is used to regulate the voltage of the DC bus capacitor constant regardless of the magnitude and direction of the rotor power. A vector control approach is used with the reference frame oriented along the stator voltage vector position. This vector position enables independent control of the active and reactive power flowing between the grid and the grid side converter [47]. Figure 5.7 shows the schematic of the grid side converter.

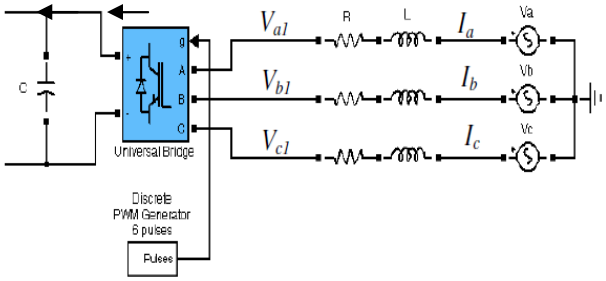

Figure 5.7 Schematic Diagram of the Grid Side Converter

The voltage across the inductors is represented as

$$\begin{bmatrix} V_a \\ V_b \\ V_c \end{bmatrix} = R\begin{bmatrix} I_a \\ I_b \\ I_b \end{bmatrix} + L\frac{d}{dt}\begin{bmatrix} I_a \\ I_b \\ I_b \end{bmatrix} + \begin{bmatrix} V_{a1} \\ V_{b1} \\ V_{c1} \end{bmatrix} \tag{5.8}$$

Where L and R are the line inductance and resistance, respectively.

Using Park's transformations, the voltage equations on d-q reference frame rotating at ω_e can be represented:

$$\begin{bmatrix} V_d \\ V_q \end{bmatrix} = R\begin{bmatrix} I_d \\ I_q \end{bmatrix} + L\frac{d}{dt}\begin{bmatrix} I_d \\ I_q \end{bmatrix} + \omega_e L\begin{bmatrix} -I_q \\ I_d \end{bmatrix} + \begin{bmatrix} V_{d1} \\ V_{q1} \end{bmatrix} \tag{5.9}$$

The angular position of the voltage is calculated as:

$$\theta_e = \int \omega_e dt = \tan^{-1}(\frac{V_\beta}{V_\alpha}) \tag{5.10}$$

where V_α, V_β are the stator voltage components on the stationary reference frame.

The active and reactive power flow is calculated as:

$$\begin{aligned} P &= V_d I_d + V_q I_q \\ Q &= V_d I_q + V_q I_d \end{aligned} \tag{5.11}$$

Aligning the d-axis of the reference frame along the stator voltage position given by equation (5.10), $V_q = 0$ and V_d is constant and equal to the amplitude of the grid voltage. The active and reactive power will be proportional to I_d and I_q, respectively. Neglecting effects of high frequency switching and the losses in the inductor, it is seen that the DC voltage can be controlled via I_d by exchanging active power with the grid to charge the capacitor. Figure 5.8 shows the vector control structure for grid side converter.

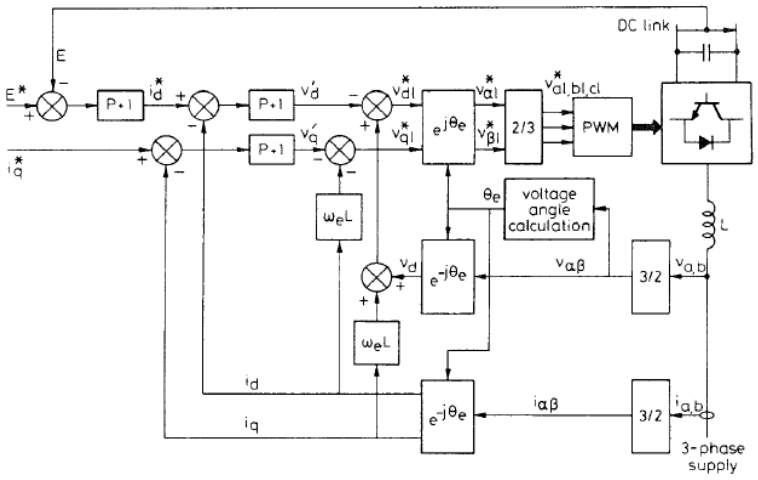

Figure 5.8 Vector Control Structure for Grid Side Converter Controller

By applying the phase lock loop technique (PLL), the reference voltage angle of the signal (θ_e) can be determined. An outer regulation loop consists of a DC voltage regulator and an inner current regulation loop consists of a current regulator. The current regulator controls the magnitude and phase of the voltage generated by grid side converter from the i_d^* commanded by the DC voltage regulator. The current regulator is assisted by feed-forward terms which transfer to the output voltage reference. The PWM converter is considered as a current-controlled voltage source converter.

5.6.2. Conventional Rotor Side Inverter

The main goal of the rotor side inverter is to control independently the active and reactive power. The power is controlled indirectly by controlling the rotor current. In this control scheme, the rotor side inverter is controlled in a synchronously rotating d-q axis reference frame, with the d-axis oriented along the stator-flux vector position as shown in Figure 5.9. In this way, a decoupled control between the electrical torque and the rotor excitation current is also obtained [47].

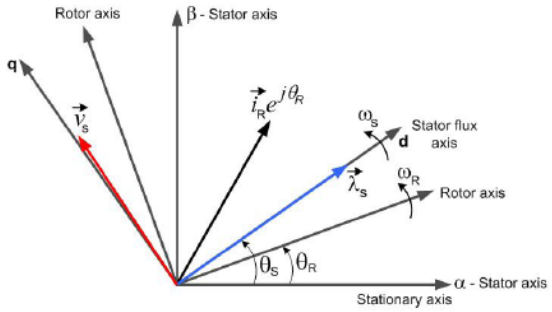

Figure 5.9 Vector Diagram in d-q Reference Frame considering a Field Oriented Control

According to this vector orientation, it can be concluded that:

$$\begin{aligned} \lambda_{sq} &= 0\ ,\ \lambda_{sd} = \left|\lambda_s\right| \\ V_{sd} &\approx 0\ ,\ V_{sq} = \left|V_s\right| \end{aligned} \tag{5.12}$$

Substituting these relationships into Equation 5.6, the power equations will result in:

$$\begin{aligned} P_s &= \frac{3}{2}(V_{sq} i_{sq}) \\ Q_S &= \frac{3}{2}(V_{sd} i_{sd}) \end{aligned} \tag{5.13}$$

The above equations show that active and reactive power of the stator can be controlled independently via the current components. Hence, the rotor current reference on d-q axis can be represented as follows;

$$\begin{aligned} i_{rq,ref} &= -\frac{L_s}{V_s L_m} P_{S,ref} \\ i_{rd,ref} &= \frac{\lambda_s}{L_m} - \frac{L_s}{V_s L_m} Q_{S,ref} \end{aligned} \tag{5.14}$$

Figure 5.10 shows a schematic block diagram for a vector control structure for a conventional rotor side inverter controller. The active power control contains two control loops in cascade: a slower (outer) power control loop and a fast (inner) rotor current control loop. The slower power control loop has thus as output the reference rotor current signal, which is used further by the fast current control loop. The rotor side inverter provides the actuation, and the

control requires the measurement of the stator and rotor currents, stator voltage and the rotor position. It is also important to note that VR and T represent rotation and phase transformations, respectively.

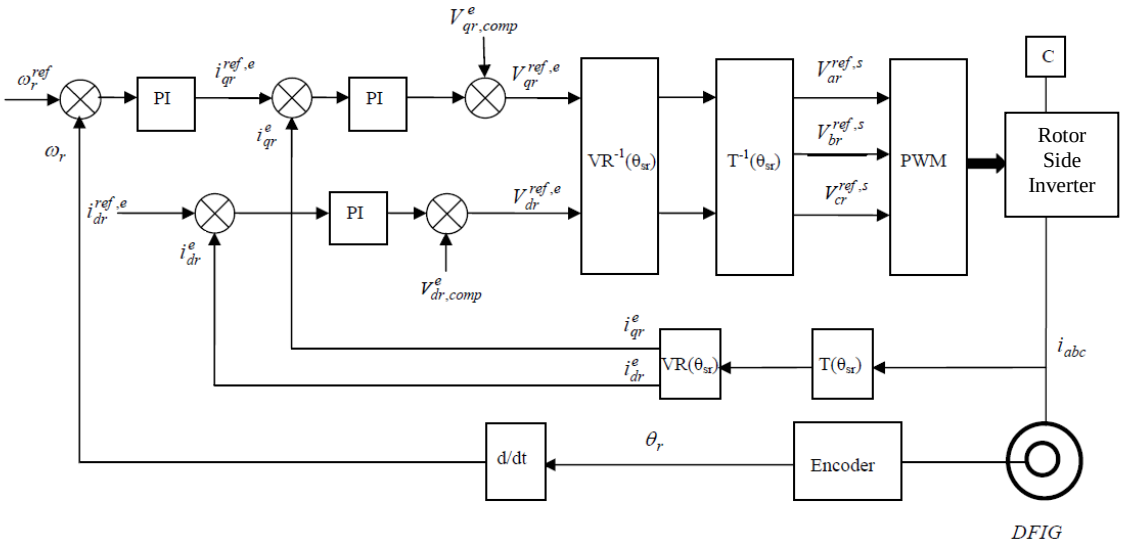

Figure 5.10 Vector Control Structure for Conventional Rotor Side Inverter Controller

5.7 Summary

From the above analytical expression and theoretical study of machine dynamic behavior, we can conclude that the normal power control can be achieved from the conventional rotor side inverter by controlling from the rotor currents on both d-q axis reference frame where the speed reference can be determined from a power-speed characteristic curve. The rotor voltages will be responsible of controlling the DFIG during normal operation. However, this conventional controller is incapable of dealing with rotor imbalance disturbance. As a consequence, oscillation will be produced from the wind turbine and result in an effect on the current both the stator side and the rotor side during this kind of situation. This will lead to wind output power quality problems. Therefore, improving its behavior during rotor imbalance disturbance has become the main objective for this dissertation.

CHAPTER 6

THE PROPOSED ROTOR SIDE INVERTER CONTROLLER

The proposed method intends to design a control strategy using the rotor side inverter to help reduce the oscillation of the wind turbine's output when rotor imbalance affects the generator. The current control approach considering a vector oriented control (VOC) philosophy in the d-q reference frame is applied. This is useful in order to reduce the complexity of the DFIG mathematical equation from Park's transformation. This control technique reduces the oscillation of wind turbine output by control from rotor side, which requires lower power injection compared with the grid side converter, and no extra hardware is required. The feasibility of this design has been proven by means of a mathematical model and digital simulations based on Matlab/Simulink [48].

6.1 The Proposed Control Structure of the Rotor Side Inverter Controller

The layout of the proposed control structure of the rotor side inverter controller is shown in Figure 6.1. The current control approach considering a vector oriented control (VOC) philosophy in the d-q reference frame is applied. As depicted in Figure 6.1, under normal power-speed control from wind turbine control level and combining the stator flux amplitude/phase angle estimator with oscillating current extraction, the current components at the oscillating frequency were extracted. This rotor current is also used to estimate the next sampling stator side current in order to better perform the current control. Modification of decoupling voltage control makes it possible to obtain the estimated rotor voltage that is needed to inject the desired current into the DFIG via the current-controlled voltage source PWM inverter.

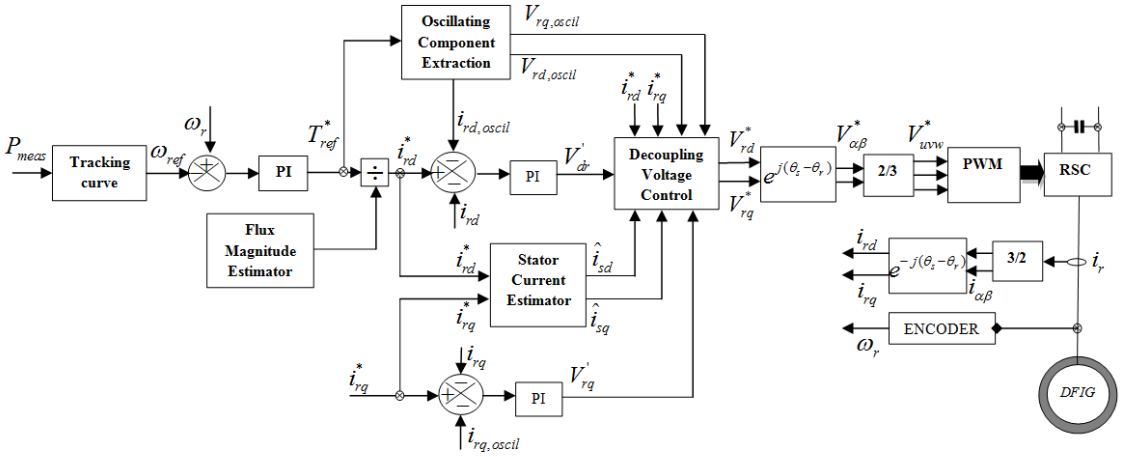

Figure 6.1 Proposed Control Structure of Rotor Side Inverter Controller

6.2 Stator Flux Magnitude and Phase Angle Estimation

From the coordinate of stator flux on d-q reference frame in Figure 5.9, the expression of the stator flux magnitude ($|\lambda_s|$) can be defined as

$$\begin{aligned} \lambda_{sd} &= \int (V_{sd} - R_s i_{sd})dt \\ \lambda_{sq} &= \int (V_{sq} - R_s i_{sq})dt \\ |\lambda_s| &= \sqrt{(\lambda_{sd})^2 + (\lambda_{sq})^2} \end{aligned} \tag{6.1}$$

The phase angle (θ_e) is calculated by

$$\theta_e = \tan^{-1}\frac{\lambda_{sq}}{\lambda_{sd}} \tag{6.2}$$

6.3 Oscillating Rotor Current Extraction

In order to keep all other frequency current components, the frequency-varying band-pass filter is used to extract only the oscillating current component at a particular frequency. This will come to effect only in the presence of the rotor imbalance. It is designed to have large gain at the known disturbance frequency (oscillating frequency) but also have a negligible effect at all other frequencies. The oscillating frequency can be determined by the fault detection

presented in Chapter 3. This current extraction is done by using a high-Q second order band-pass filter.

For a second-order low bandwidth band-pass filter the transfer function is given by

$$H(s) = \frac{H_0 \beta s}{s^2 + \beta s + \omega_0^2} = \frac{s\omega_0 / Q_{filt}}{s^2 + s\omega_0 / Q_{filt} + \omega_0^2} \tag{6.3}$$

where β is Bandwidth

$\omega_0 = 2\pi f_0$ is Center/Natural frequency

H_0 is Maximum amplitude of the filter

The frequency response of second order band-pass filter is illustrated in Figure 6.2.

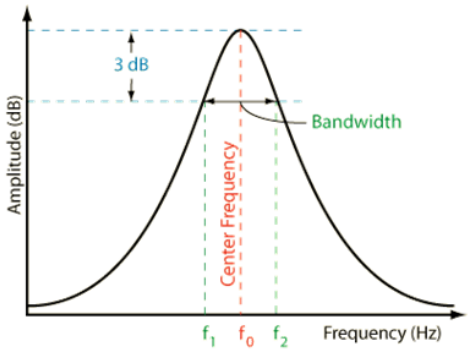

Figure 6.2 Frequency Response of the Low Bandwidth Second Order Band-Pass Filter

6.4 Stator Side Current Estimation

This section will be devoted to the mathematical modeling of the DFIG [49]. The objective of this part will be focused on finding a relationship between the state space variables that could permit prediction of the behavior of the DFIG under disturbance conditions. Since the aim of this research is to suppress the vibration which causes the harmonics at a certain frequency of stator current, this event is considered as one kind of disturbance. In order to operate this proposed rotor side inverter controller during this event, the stator side current estimator is integrated into this controller. This analysis will constitute the basis for the design of the control system for the rotor side inverter controller.

The current estimator will predict the dynamic stator current in a d-q rotating reference frame by estimating the stator current vector from the rotor side current vector. The predicted output response of the stator current should be closed to the real stator current and should have fast dynamic response. Once the stator current vector is correctly estimated by calculating from the rotor side current vector, any unwanted signal due to disturbance can be suppressed by applying proper controlling signals from the rotor side inverter.

First, considering that the dynamic voltage equation of the rotor is linear and assuming that the magnetic circuit of DFIG is linear, by applying the Laplace transformation, we can obtain the stator current on the d-q rotating frame as follows;

$$\begin{aligned} i_{sd} &= \frac{(L_s s + R_s).V_{sd} + \omega_s L_s V_{sq}}{L_s^2 s^2 + 2L_s R_s s + R_s^2 + \omega_s^2 L_s^2} - \frac{(L_s s^2 + R_s s + \omega_s^2 L_s) L_m i_{rd} - R_s \omega_s L_m i_{rq}}{L_s^2 s^2 + 2L_s R_s s + R_s^2 + \omega_s^2 L_s^2} \\ i_{qs} &= \frac{(L_s s + R_s).V_{qs} - \omega_s L_s V_{sd}}{L_s^2 s^2 + 2L_s R_s s + R_s^2 + \omega_s^2 L_s^2} - \frac{(L_s s^2 + R_s s + \omega_s^2 L_s) L_m i_{rq} + R_s \omega_s L_m i_{rd}}{L_s^2 s^2 + 2L_s R_s s + R_s^2 + \omega_s^2 L_s^2} \end{aligned} \quad (6.4)$$

The equations 6.4 can be simplified considering that the stator flux is aligned with the d-q reference frame in a field oriented control system, and hence its quadrature component is null. Besides, assuming that the leakage inductance value is low, the stator voltage vector can be considered to be almost aligned with the q-axis. In this manner, the previous equations can be written as:

$$\begin{aligned} i_{sd} &= \frac{1}{L_s} \frac{\omega_s}{(s^2 + 2(\frac{R_s}{L_s})s + \omega_s^2)} V_{sq} - \frac{L_m}{L_s} i_{rd} \\ i_{sq} &= \frac{1}{L_s} \frac{s + (\frac{R_s}{L_s})}{(s^2 + 2(\frac{R_s}{L_s})s + \omega_s^2)} V_{sq} - \frac{L_m}{L_s} i_{rq} \end{aligned} \quad (6.5)$$

The equation 6.5 shows the variation in the stator voltage and rotor current introduce oscillations in the d-q components of the stator currents in the synchronous reference frame.

The frequency of such oscillation is equal to once per revolution of the rotating part of the DFIG. This phenomenon can be specially noticed during rotor imbalance conditions.

In the steady state, the current in the stator windings can be written as:

$$\begin{aligned} i_{sd} &= \frac{1}{\omega_s L_s} V_{sq} - \frac{L_m}{L_s} i_{rd} \\ i_{sq} &= \frac{R_s}{\omega_s^2 L_s^2} V_{sq} - \frac{L_m}{L_s} i_{rq} \end{aligned} \tag{6.6}$$

From the above equation, since the inductive reactance is much greater than the stator resistance it can be concluded that the stator's voltage term tends to zero. This equation can be reduced and the predicted stator current on d-q component ($\hat{i}_{sd}, \hat{i}_{sq}$) as shown below:

$$\begin{aligned} \hat{i}_{sd} &= \frac{1}{\omega_s L_s} V_{sq} - \frac{L_m}{L_s} i_{rd} \\ \hat{i}_{sq} &= -\frac{L_m}{L_s} i_{rq} \end{aligned} \tag{6.7}$$

From equation 6.7, we see that the final value of stator current $\hat{i}_{sd}$ depends upon two terms. The first one, considering the steady state conditions, describes its relationship with the magnetization's current, while the second term depends on the rotor d-axis current component. On the other hand, there is also linear dependence between the stator and rotor current components on the q-axis.

6.5 Modified Decoupling Voltage Control

The aim of this analysis is to control the d-q current components carried out for the rotor side inverter. Using a stator flux-oriented approach, implementation with the current-controlled PWM converter requires a decoupling control scheme [50]. From equation 6.8, we can see that this system is coupled because the inductance matrix is not diagonal. This means that any changes on voltage components in the d-q axis will result in changes in both d-q current components.

$$\begin{bmatrix} \lambda_{ds} \\ \lambda_{qs} \\ \lambda_{dr} \\ \lambda_{qr} \end{bmatrix} = \begin{bmatrix} L_s & 0 & L_m & 0 \\ 0 & L_s & 0 & L_m \\ L_m & 0 & L_r & 0 \\ 0 & L_m & 0 & L_r \end{bmatrix} \begin{bmatrix} i_{ds} \\ i_{qs} \\ i_{dr} \\ i_{qr} \end{bmatrix} \tag{6.8}$$

In order to get rid of this problem, the voltage equations will be redeveloped to compensate for the cross coupling between d-q axes, by defining the leakage factor of the induction machines as

$$\sigma = 1 - \frac{L_m^2}{(L_{ls} + L_m)(L_{lr} + L_m)} \tag{6.9}$$

Substituting this leakage factor equation into rotor flux equations:

$$\begin{aligned} \lambda_{rd} &= \sigma L_s i_{rd} + \frac{L_m}{L_s} \lambda_{sd} \\ \lambda_{rq} &= \sigma L_r i_{rq} \end{aligned} \tag{6.10}$$

Applying these flux equations and rearranging the d-q rotor voltage equations, we obtain the following;

$$\begin{aligned} V_{rd} &= R_r i_{rd} + \sigma L_r \frac{di_{rd}}{dt} - \omega_{slip} \sigma L_r i_{rq} \\ V_{rq} &= R_r i_{rq} + \sigma L_r \frac{di_{rq}}{dt} + \omega_{slip} (\sigma L_m i_{ms} + \sigma L_r i_{rd}) \end{aligned} \tag{6.11}$$

The current errors on both d-q components are processed by PI controller to give $V_{rd}^{'}$, V'_{rq} respectively. This voltage output can be formed as follow;

$$\begin{aligned} V_{rd}^{'} &= R_r i_{rd} + \sigma L_r \frac{di_{rd}}{dt} \\ V_{rq}^{'} &= R_r i_{rq} + \sigma L_r \frac{di_{rq}}{dt} \end{aligned} \tag{6.12}$$

Since this system needs to adapt to disturbance condition and we want to ensure good tracking of the current control with fast dynamic response, the above decoupling voltage equations need to be modified.

In order to perform a better current control and obtain a more accurate reference voltage command, the compensation terms are added to the reference voltages, making it possible to achieve decoupled performance of stator flux-oriented control of rotor side inverter controller. The predicted stator current which estimated from rotor side current components will also be taken into account. In order to eliminate the harmonics of current components at the oscillating frequency, the compensation voltage calculated from oscillating current extraction will be added.

Finally, the modified reference voltages command (V_{rd}^{*}, V_{rq}^{*}) can be represented in these following equations;

$$\begin{aligned} V_{rd}^{*} &= V_{rd}^{'} + i_{rd}^{*} R_r - \omega_{slip}(L_r i_{rd}^{*} + L_m \hat{i}_{sd}) + i_{rd\_oscill} R_r \\ V_{rq}^{*} &= V_{rq}^{'} + i_{rq}^{*} R_r + \omega_{slip}(L_r i_{rq}^{*} + L_m \hat{i}_{sq}) + i_{rd\_oscill} \omega_{slip} L_r \end{aligned} \tag{6.13}$$

As mentioned, a current-controlled voltage source PWM inverter is chosen in this study. In order to control the generator current output, this inverter will force the rotor current to follow their reference signals in both on d-q reference frame via the required reference voltages (V_{rd}^{*}, V_{rq}^{*}) by injecting at the rotor windings. By comparing desired and actual values of the current from measurement, this current-controlled inverter generates the switching states for the switches in order to decrease the current output error. Therefore we can obtain the suitable switching signals to control the output current as commanded.

6.6 Simulation Setup

The proposed control of the rotor side inverter was verified on a 9MW wind farm with GE1.5MW doubly fed induction generator (DFIG) through computer simulation. It is assumed that the DFIGs in the wind farm act coherently. The equivalent wind turbine model in the

simulation consists of a rotor, a gearbox, and the DFIG subsystem. All machine parameters and aerodynamic characteristic of this device are presented in Table 6.1.

Table 6.1 9-MW Wind Farm Parameters in this Study

Parameter (Unit)	Value
Nominal power (MVA)	9
Rated voltage (V)	575
Nominal frequency(Hz)	60
Stator resistance (p.u.)	0.007
Stator leakage inductance (p.u.)	0.171
Magnetizing inductance (p.u.)	2.9
Rotor resistance (p.u.)	0.005
Rotor leakage inductance (p.u.)	0.156
Number of pairs of poles	2
Nominal DC voltage (V)	1200

The system performance and capabilities of the discussed control strategy were tested under different operating conditions such as normal operation and under rotor imbalance conditions. Simulation of this proposed control strategy was carried out on MATLAB/Simulink platform. Four key events of real wind speed were used as wind speed input; constant wind speed, wind ramp up, wind ramp down, and a wind gust event. To perform the vibration suppression of the DFIG, the rotor imbalance condition is introduced into the wind turbine system. Details of the simulation results and discussion are given at the next section.

6.7 Simulation Results

6.7.1. Wind Constant Event

To perform the overall control system of proposed rotor side inverter controller, the wind turbine system will be tested under constant wind speed. The rotor imbalance condition will be introduced into the system at t=5 second and the vibration suppression scheme will later be applied at t=10 second.

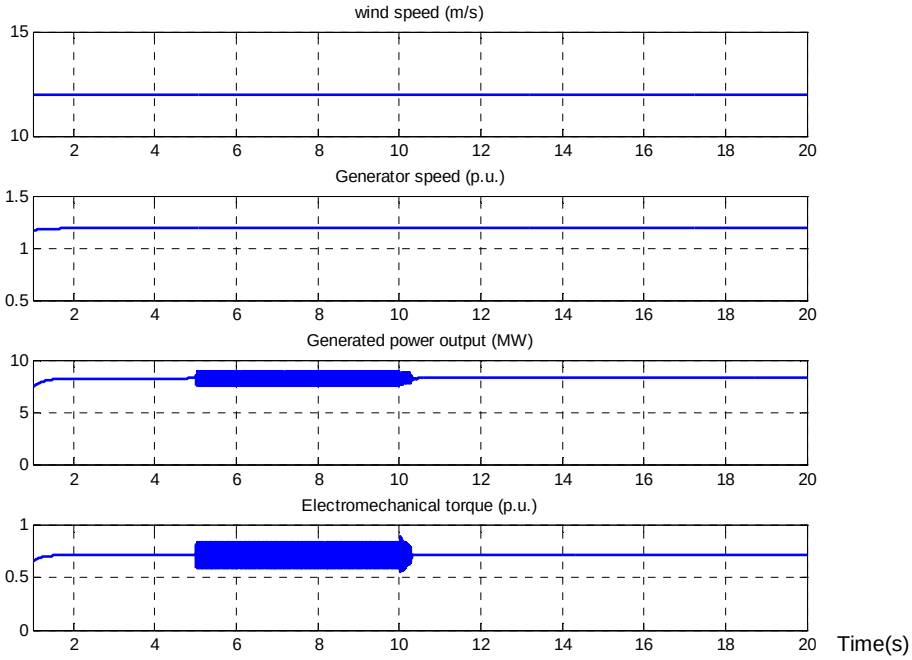

Figure 6.3 Simulation Results of Wind Speed (m/s), Generator Speed (p.u.), Generated Power Output (MW) and Electromechanical Torque (p.u.) responded on Constant Wind Event

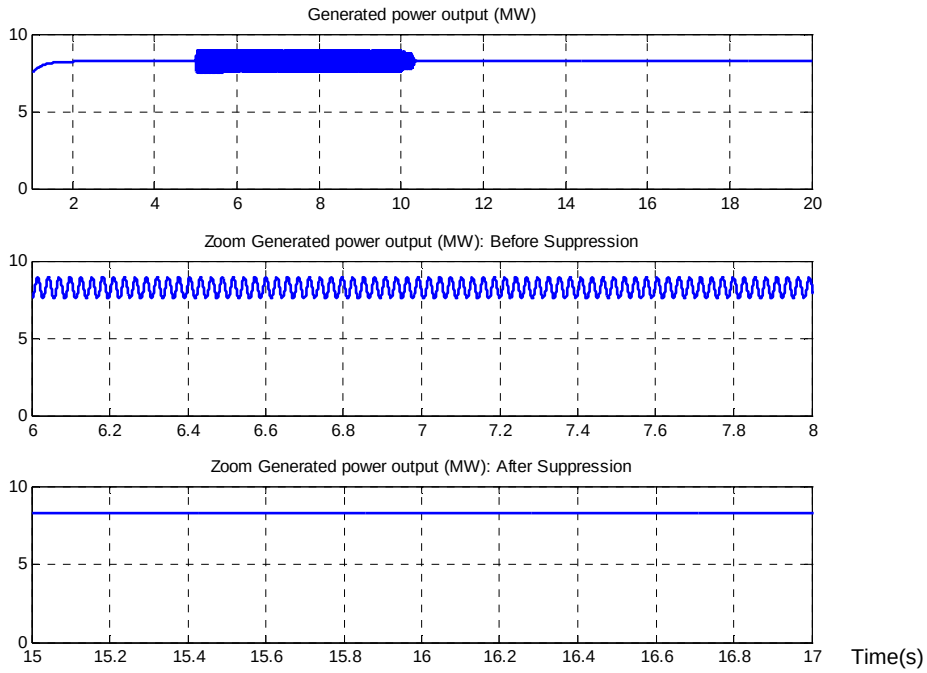

Figure 6.4 Simulation Results of Generated Power Output (MW): Before and After Suppression

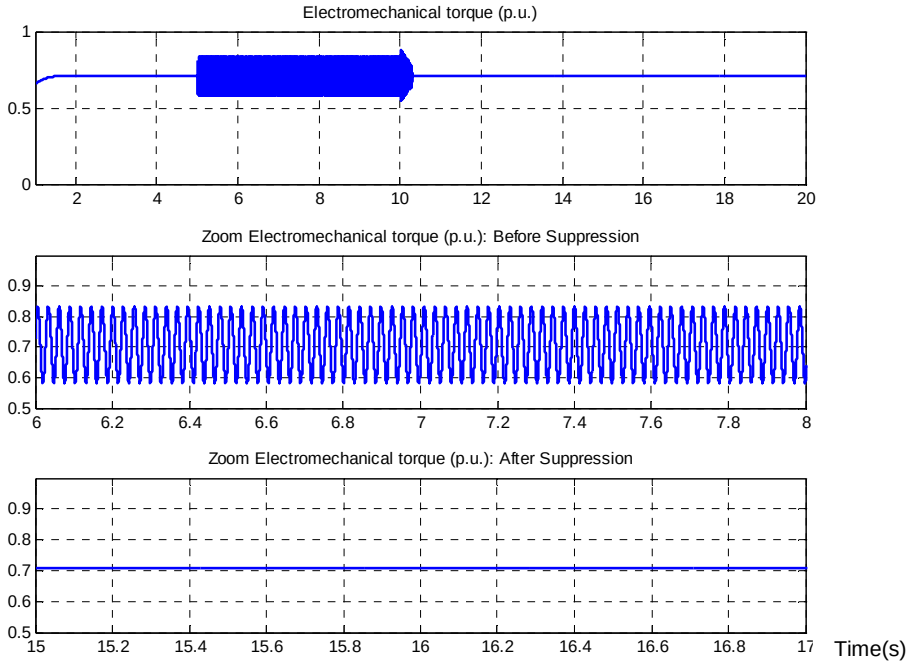

Figure 6.5 Simulation Results of Electromechanical Torque (p.u.): Before and After Suppression

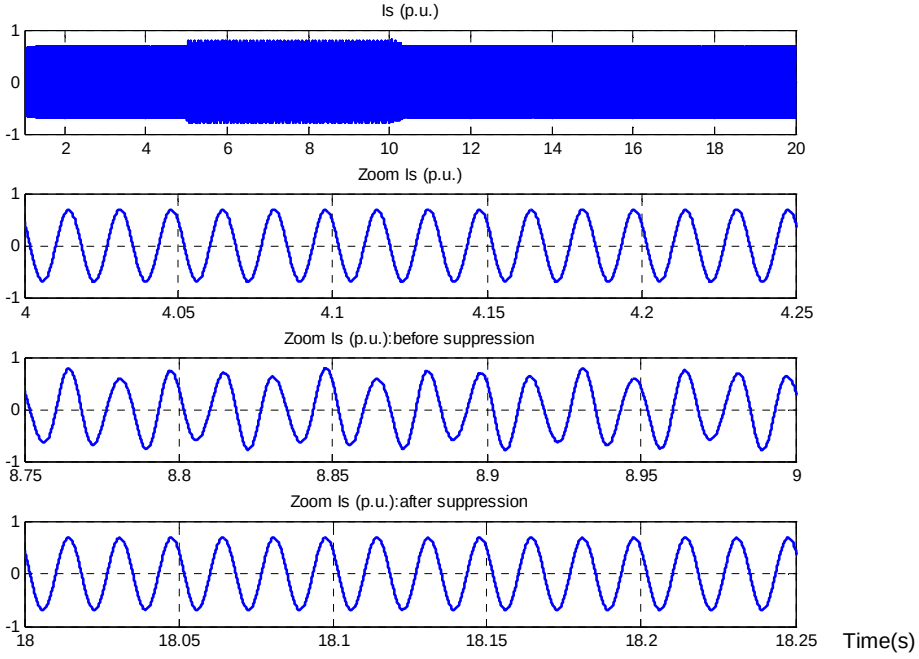

Figure 6.6 Simulation Results of Generated Current Output (p.u.) and Zoomed Versions of Current Output (p.u.): Before and After Suppression

The simulation results, depicted in Figure 6.3, show the response of the wind speed, generator speed, generated power and torque during the wind constant event. When the rotor imbalance occurs at t=5 second, the power output and torque starts to oscillate which we can see from the zoomed version results in Figure 6.4 and Figure 6.5. At t=10 second, vibration suppression scheme is applied. Figure 6.6 illustrates the DFIG behavior both before and after the suppression. The stator current flowing to the grid is back to sinusoidal waveform after suppression.

6.7.2. Instantaneous Wind Ramp up Event

As shown in Figure 6.7, on February 25th, 2008, the wind speed in the ERCOT system was suddenly ramped up and resulted in the wind generated power output jumping from 235 MW to 521 MW in 18 seconds.

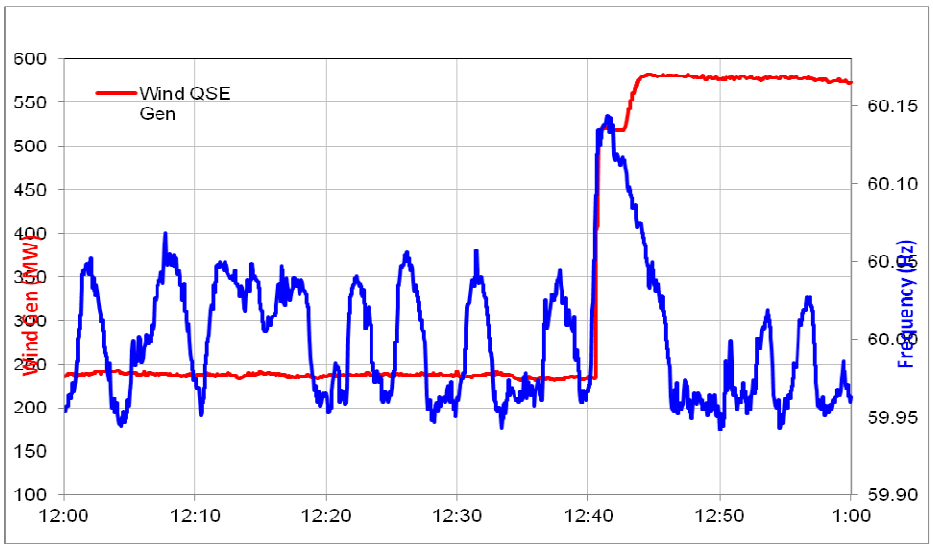

Figure 6.7 Wind Ramp up Event on February 25th, 2008

To perform the proposed control capability of rotor side inverter controller during this wind event, the rotor imbalance condition will be introduced into the system at t=5 second and the vibration suppression scheme will later be applied at t=10 second.

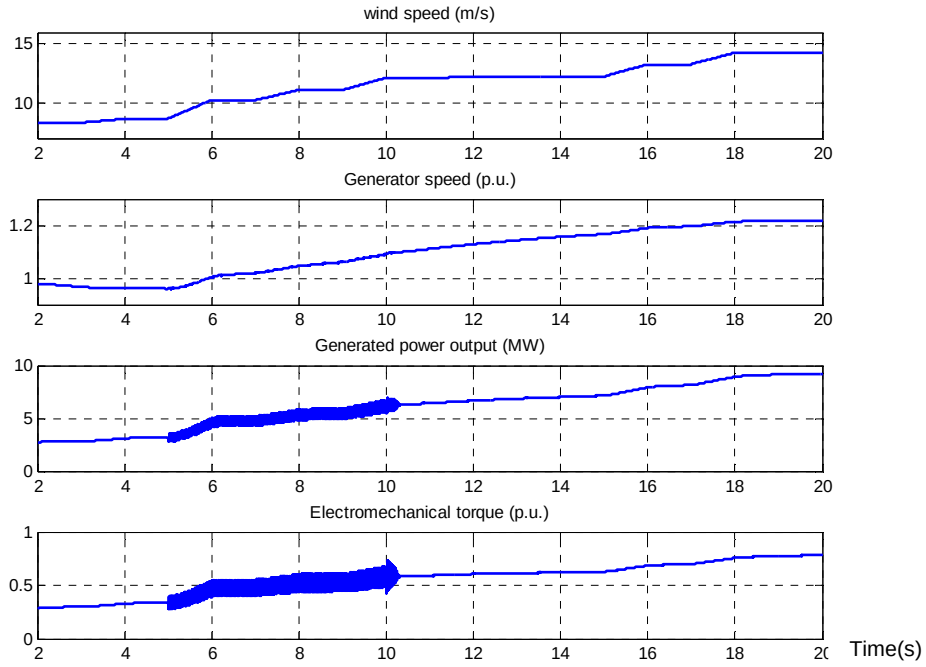

Figure 6.8 Simulation Results of Wind Speed (m/s), Generator Speed (p.u.), Generated Power Output (MW) and Electromechanical Torque (p.u.) responded on Wind Ramp up Event

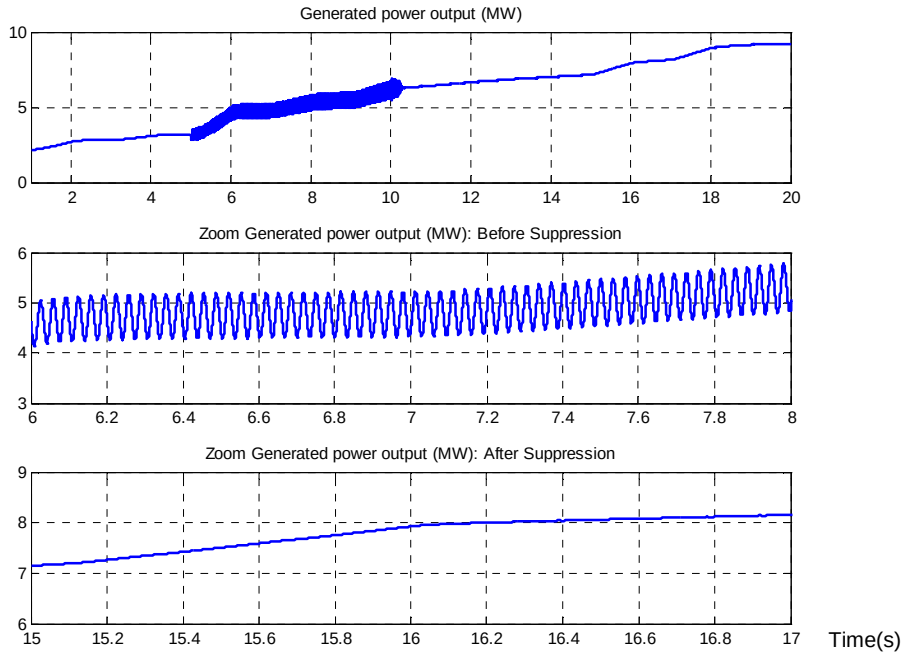

Figure 6.9 Simulation Results of Generated Power Output (MW): Before and After Suppression

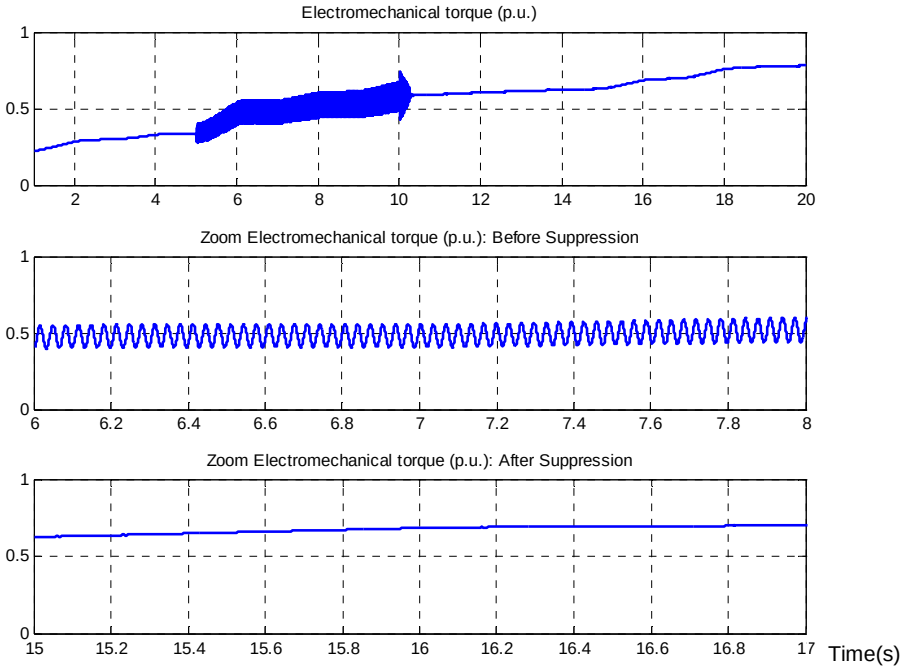

Figure 6.10 Simulation Results of Electromechanical Torque (p.u.): Before and After Suppression

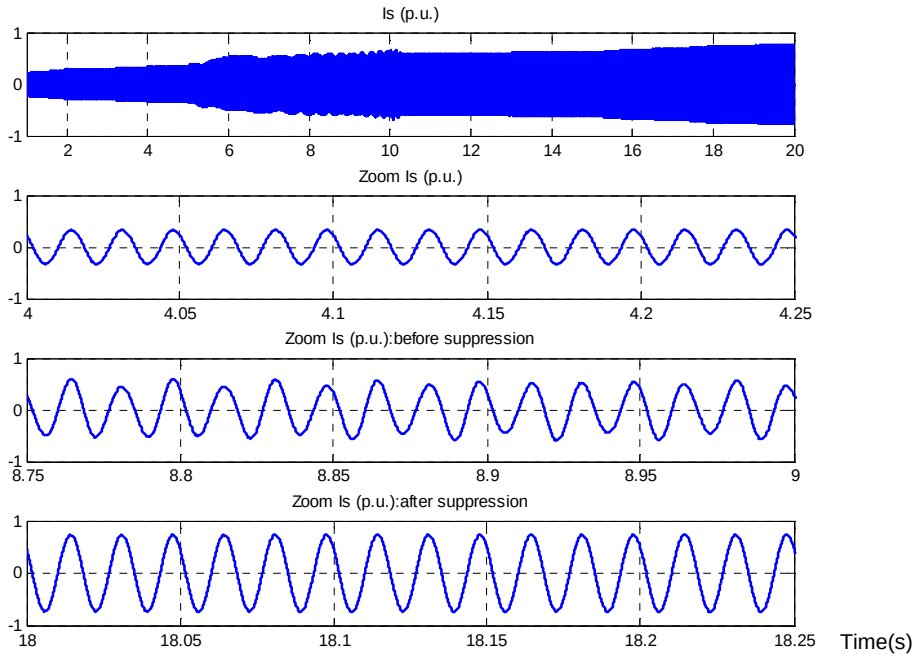

Figure 6.11 Simulation Results of Generated Current Output (p.u.) and Zoomed Versions of Current Output (p.u.): Before and After Suppression

The simulation results, depicted in Figure 6.8, show the response of the wind speed, generator speed, generated power and torque during the wind ramp up event. When the rotor imbalance occurs at t=5 second, the power output and torque starts to oscillate which we can see from the zoomed version results in Figure 6.9 and Figure 6.10. The oscillating frequency varies due to the real wind speed. Later at t=10 second, vibration suppression scheme is applied. The control system takes less than 500 ms to control the current of the stator side. Figure 6.11 illustrates the DFIG behavior both before and after the suppression. The stator current flowing to the grid is back to sinusoidal waveform after suppression. The simulations confirm effectiveness of the proposed scheme during the wind ramp up event.

6.7.3. Instantaneous Wind Ramp down Event

As shown in Figure 6.12, on February 28th, 2008, the wind speed in the ERCOT system was suddenly ramped down and resulted in a wind generated power output decrease of 243 MW in 14 seconds.

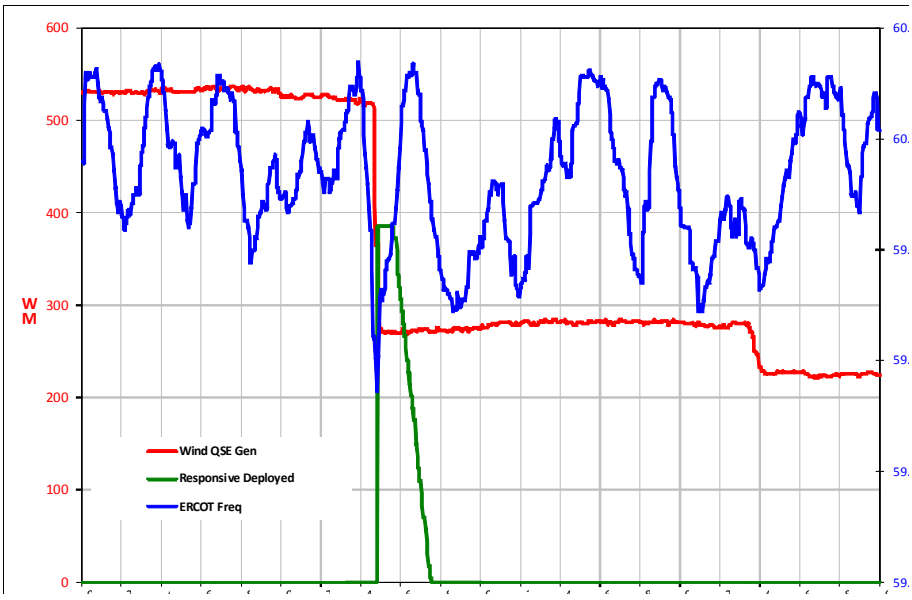

Figure 6.12 Wind Ramp down Event on February 28th, 2008

To perform the proposed control capability, the rotor imbalance conditions will introduce at t=5 second and the vibration suppression scheme will be applied at t=10 second.

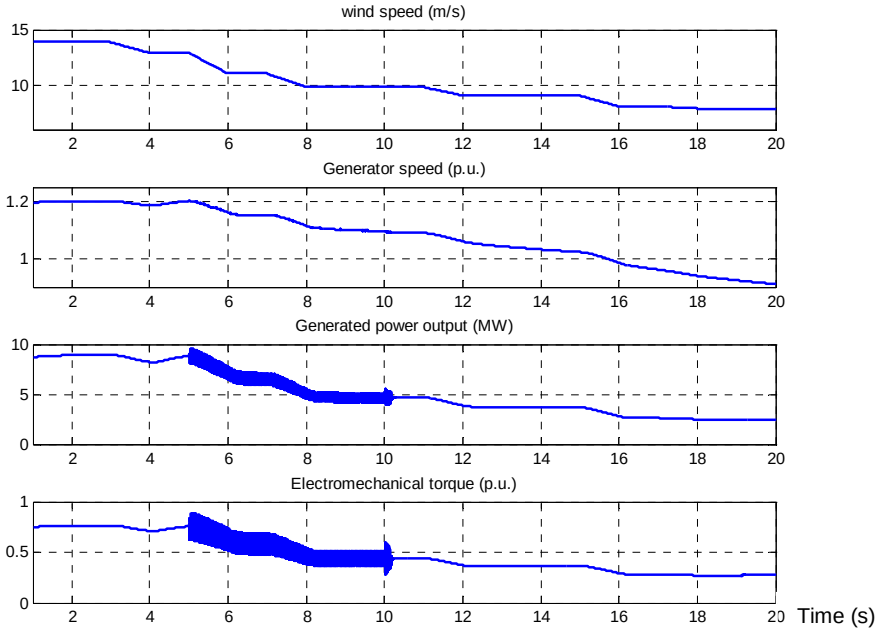

Figure 6.13 Simulation Results of Wind Speed (m/s), Generator Speed (p.u.), Generated Power Output (MW) and Electromechanical Torque (p.u.) responded on Wind Ramp down Event

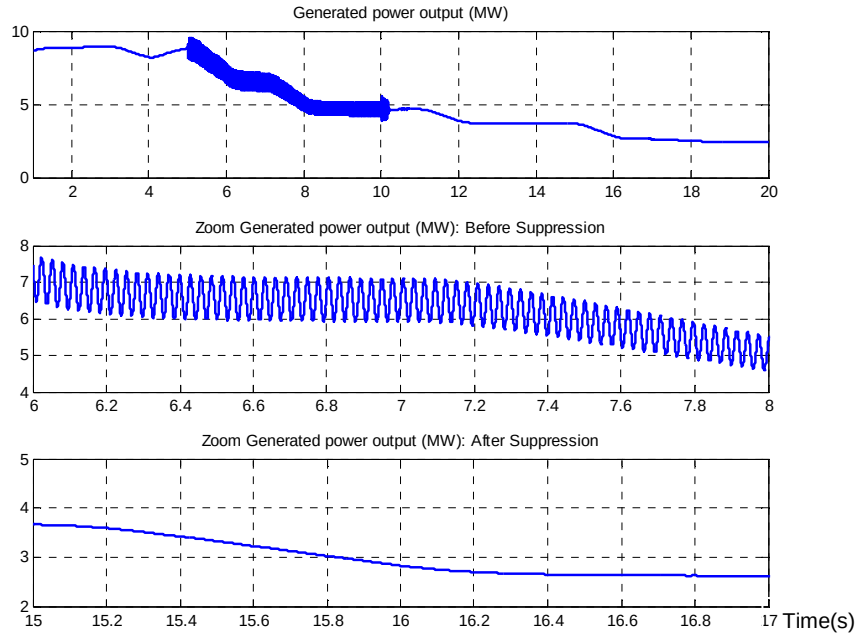

Figure 6.14 Simulation Results of Generated Power Output (MW): Before and After Suppression

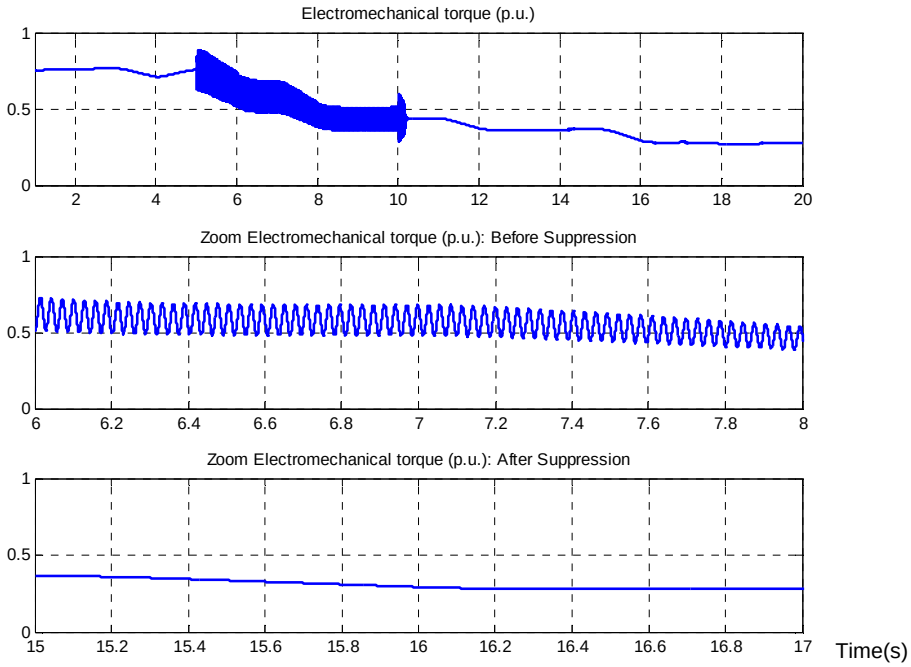

Figure 6.15 Simulation Results of Electromechanical Torque (p.u.): Before and After Suppression

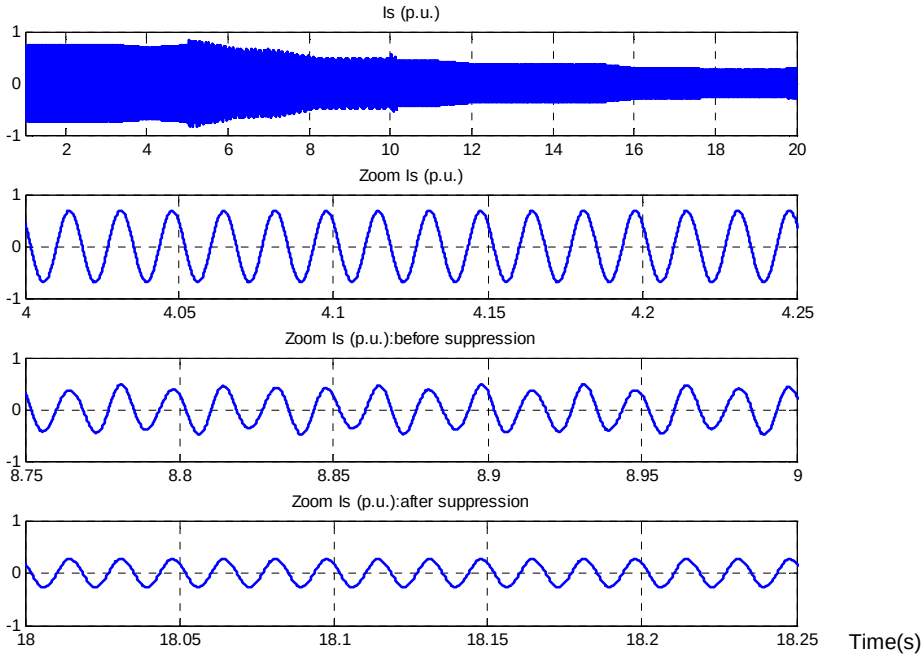

Figure 6.16 Simulation Results of Generated Current Output (p.u.) and Zoomed Versions of Current Output (p.u.) versus Time (s): Before and After Suppression

The simulation results, depicted in Figure 6.13, show the response of the wind speed, generator speed, generated power and torque during the wind ramp down event. Under the wind turbine control level, we can see that the wind turbine can perform following the wind speed profile. When the rotor imbalance occurs at t=5 second, the power output and torque starts to oscillate which we can see from the zoomed version results in Figure 6.14 and Figure 6.15. In Figure 6.16, we can see that after suppression, the stator current flowing to the grid is back to sinusoidal waveform. The simulations confirm that the proposed scheme performs well during the wind ramp down event.

6.7.4. Wind Gust Event

As shown in Figure 6.17, real wind speed data on March 4th, 2008 is used as a wind gust event input. High fluctuation of this real wind speed occurred during 11:39 PM until 12:08 AM and a 30-second time interval was selected and simulated. The minimum and maximum wind speed during this period is 8.25 m/s and 12.58 m/s, respectively.

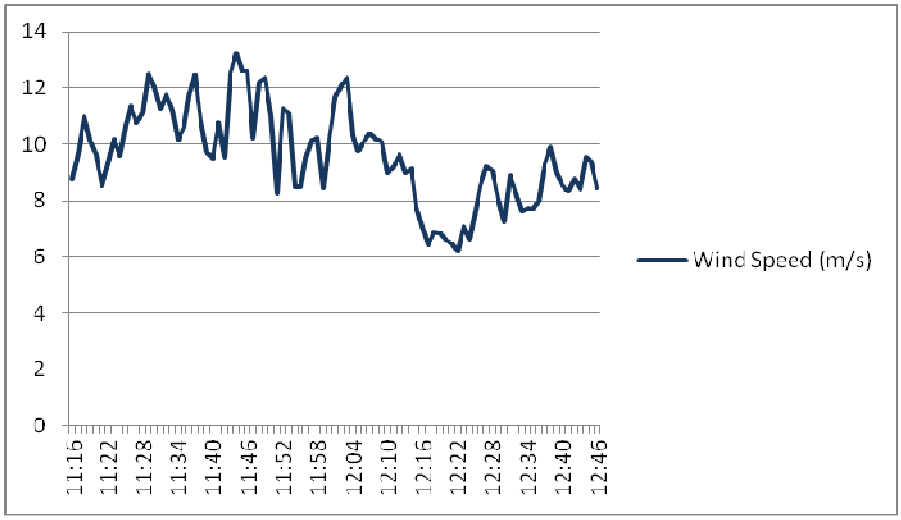

Figure 6.17 Wind Gust Event on March 4th, 2008

To demonstrate the control capability of the proposed rotor side inverter controller during this wind event, the rotor imbalance condition is introduced at t=10 second and the vibration suppression scheme will be applied at t=20 second.

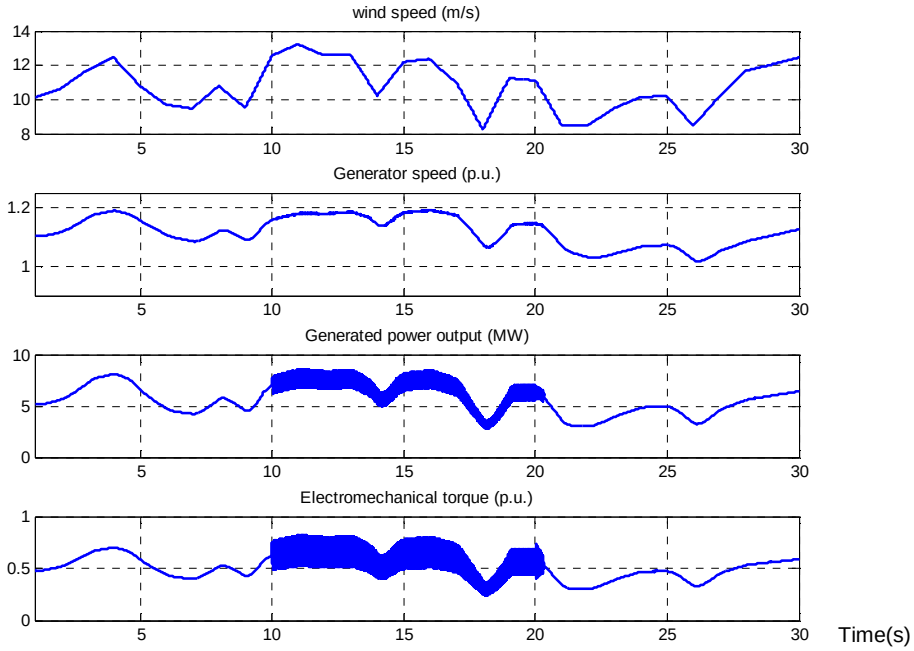

Figure 6.18 Simulation Results of Wind Speed (m/s), Generator Speed (p.u.), Generated Power Output (MW) and Electromechanical Torque (p.u.) responded on Wind Gust Event

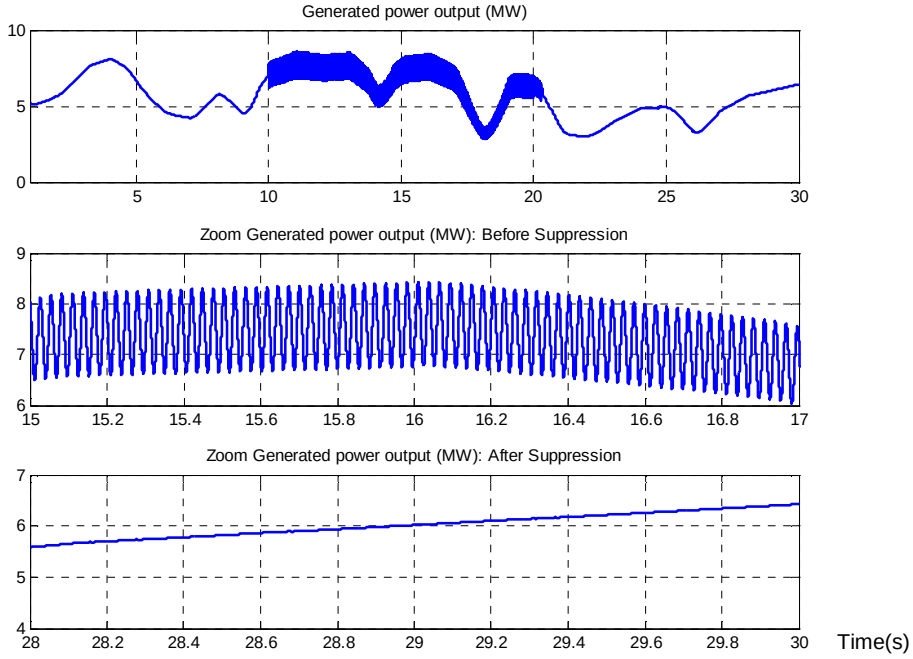

Figure 6.19 Simulation Results of Generated Power Output (MW): Before and After Suppression

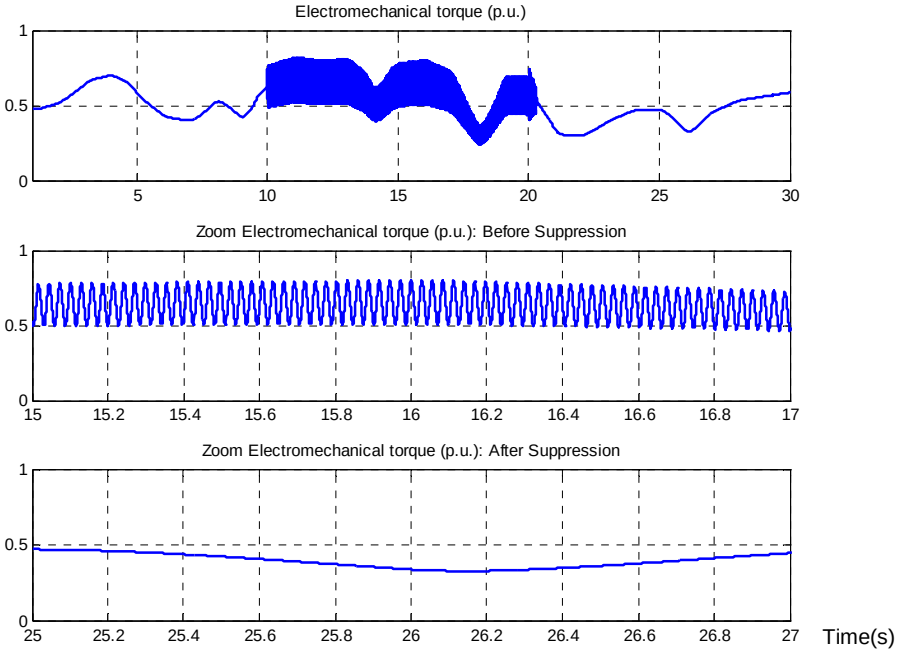

Figure 6.20 Simulation Results of Electromechanical Torque (p.u.): Before and After Suppression

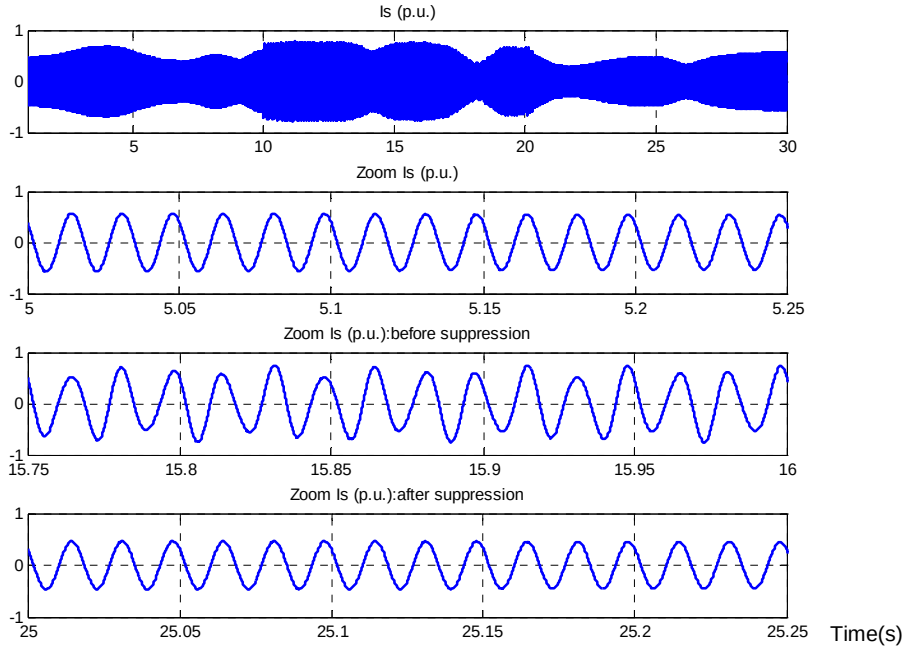

Figure 6.21 Simulation Results of Generated Current Output (p.u.) and Zoomed Versions of Current Output (p.u.): Before and After Suppression

The simulation results, depicted in Figure 6.18, show the response of the wind speed, generator speed, generated power and torque during the wind gust event. When the rotor imbalance occurs at t=10 second, the power output and torque starts to oscillate which we can see from the zoomed version results in Figure 6.15 and Figure 6.19. Figure 6.20 illustrates the DFIG behavior both before and after suppression. At t=21second after suppression, the stator current flowing to the grid is back to sinusoidal waveform. One can see that the proposed control scheme operates properly during the wind gust event.

6.8 Summary

The results show that the DFIG is able to extract the maximum power by tracking the power speed characteristic. The power and torque output have the same behavior. When a rotor imbalance happens in the wind turbine system, the output signals such as power, torque and current will oscillate at the rotational frequency under traditional control scheme. This can be seen directly from the simulation results.

Once the vibration suppression scheme is introduced into the system, the oscillation of the power and current waveform is significantly improved. The ripple of active power signal also decreases. The rotor speed and generated torque show the same behavior after the suppression scheme is applied. This control takes less than 500 ms to get into the steady state region. At the steady state response region, DFIG can recovery back to normal operation where the stator current is back to sinusoidal waveform. The power and torque output waveform also show less ripple. Four different cases of wind speed from the ERCOT system were performed to test the performance and capabilities of the control scheme. The simulation results show the effectiveness of this proposed rotor side inverter controller.

CHAPTER 7

CONCLUSIONS AND FUTURE RESEARCH

7.1 Conclusions

One of the most serious problems in wind turbines is the possibility of mechanical failure caused by rotor imbalance conditions especially for rotating parts of gears and generators. Therefore, a machine health monitoring system is a very important tool in wind turbines. Moreover, wireless sensor technologies make it possible to measure and control the vibrations of the machine during operation.

The methods of rotor imbalance detection through vibration analysis have been analyzed and assessed based on their ability to detect machine abnormalities. By using an MEMS accelerometer which is low cost, light in weight, compact in size and low in power consumption, a vibration detection method is proposed in this dissertation. Machine vibration analysis in time and frequency domain has been analyzed and a severity detection technique is also established. These are the essential components for an advance health monitoring system. The implementation of a rotor imbalance indicator can be used to estimate the range of severity levels, which makes it possible to detect the abnormalities before failure. It is very useful part of the condition based predictive maintenance.

In order to achieve better quality in wind turbine power output during rotor imbalance conditions, a new design for the rotor side inverter controller is proposed. The current control by vector oriented control (VOC) philosophy in the d-q reference frame is applied. This helps to reduce the complexity of the DFIG mathematical equation from Park's transformation. This control technique reduces the oscillation of the wind turbine output by means of control from the rotor side, which requires lower power injection compared with the grid side converter;

furthermore, no extra hardware required. The feasibility of this design has been proven by means of a mathematical model and digital simulations based on Matlab/Simulink.

It can be concluded that the proposed rotor side inverter controller is very effective at compensating for the wind power output oscillation that normally occurs when there is high machine vibration, and this control technique works well both under the normal and disturbance operation. This enhancement of the vibration suppression capabilities opens up the possibility of improving the performance of the available rotor side inverter. This will greatly improve the power quality and reduce the downtime when there is wear and tear on the mechanical components, such as shaft, gear box, and rotating parts of the DFIG before performing necessary measures to correct the issue.

7.2 Dissertation Contributions

This study presents a novel wireless health monitoring and control system for wind turbine systems to detect the severity level of rotor imbalance conditions of the generator. Moreover, a new design of the rotor side inverter is proposed to reduce the oscillation of the wind turbine output during rotor imbalance conditions. The major contributions of this dissertation are:

• Develop and implement a ZigBee based wireless sensor network for a health monitoring and control system which will be able to detect rotor imbalance conditions based on the vibration signature.

• Study and investigate rotor imbalance phenomena affecting the electrical machine by hardware testing.

• Propose and validate vibration based detection techniques to predict the level of rotor imbalance severity and be able to estimate the usable life of the equipment.

• Study the overall control system of DFIG based wind turbine and develop a machine model including the models of the AC-DC-AC converter, grid side converter, and rotor side inverter to draw maximum electrical power from the DFIG irrespective of the wind speed.

• Investigate rotor imbalance conditions affecting the DFIG, mainly focused on the quality of wind turbine output signal.

• Design and propose a control strategy for the rotor side inverter controller to reduce the oscillation of the generated wind turbine output and allow it to operate during disturbance conditions, while also providing the standard active and reactive power control.

• The feasibility of this proposed design has been proven by means of a mathematical model and computer simulations by Matlab/Simulink software. The simulation results of the proposed capability are shown to illustrate the effectiveness of the rotor side inverter controller.

7.3 Possible Future Research

As mentioned in the introductory chapter, it becomes more urgent to develop accurate condition monitoring and fault diagnosis methods due to rapid deployment of wind generations. With the existing technology used to protect wind turbine systems, condition monitoring needs signals from several sensors that are costly and difficult to install in already mounted wind turbines. At the same time, sensor failures can also reduce the wind turbine reliability.

This proposed vibration detection technique is mainly for drive train components and the rotating parts of generators. However, the rotor imbalance issues have also been shown to interact with the stochastic characteristics of aerodynamic load, wind wheel unbalance, and asymmetry in pitch angle, which limit the usage of traditional fault detection techniques. Therefore, the effects of the aforementioned factors need to be taken into account. The practice of predictive maintenance for blade pitch control systems integrated with the proposed vibration detection technique might also help achieve more accurate analysis of this detection.

Some other techniques of diagnosis and prognosis developed in the aerospace industry could also provide good references for wind turbine condition monitoring. Model-based fault diagnosis has received much attention, from the sub-system level to the whole system level. Grey-box modeling approaches appear more appropriate and thus deserve more study in the

future. The multi-agent system approach is also a good candidate for advance diagnostic and deserves more study.

To be able to operate a wind turbine during rotor imbalance conditions, the proposed rotor side inverter controller could be automatically invoked following the detection of rotor imbalance from machine health monitoring system. However, to obtain minimum transient response during the transition state of the control, the parameters of the machine and the initial conditions of the controller need more study. Estimation of machine parameters such as resistance and inductance through on-line monitoring system can give more accurate information about machine health so operators can do fine-tuning these parameters in order to avoid the overcompensated signal at the wind turbine output.

Due to the wind speed variations especially during the wind gust event, the output power of wind turbine fluctuates. This power fluctuation makes the wind power undispatchable. Furthermore, it can cause frequency deviation. This creates significant problems for grid operators that increase as the amount of installed wind power grows. In order reduce the power fluctuation lead to less power system impacts, how to smooth output power of wind generation system is very important. The control algorithms to smooth the power fluctuation during wind gust event need more study and investigation. Combining the vibration suppression scheme and power smoothing approach into the rotor side inverter may enhance more reliability and efficiency of the DFIG wind turbine control system.

APPENDIX A

SOURCE CODE

Source code of Programming the ZigBee Node

```
//*****************************************************************************
  Filename: SensorCollector_12bit_3CH.c

Target:       cc2430
Author:       Suratsavadee K.
Revised:      June 2009


  Description:  This application function either as a Coordinator/Sensor
  The role of the application is chosen within this program/sourcecode at initialisation.

  Push S1 At Coordinator -->  Sensor Start Sampling
  LED 1 (Both Coordinator/Sensor) indicates that device is powered.
  LED 2 (Sensor) indicates at the end of ADC conversion.
*****************************************************************************/

/*****************************************************************************
* INCLUDES
*/
//#include <hal_lcd.h>
#include <hal_led.h>
#include <hal_joystick.h>
#include <hal_assert.h>
#include <hal_board.h>
#include <hal_int.h>
#include "hal_mcu.h"
#include "hal_button.h"
#include "hal_rf.h"
#include "util_lcd.h"
#include "basic_rf.h"

#include "app_ex.h"
#include <string.h>
#include <stdio.h>

/*****************************************************************************
* CONSTANTS
*/
// Application parameters
#define RF_CHANNEL              25      // 2.4 GHz RF channel

// BasicRF address definitions
#define PAN_ID              0x2007
#define SWITCH_ADDR         0x2510

#define NODE5_ADDR          0x2550


#define APP_PAYLOAD_LENGTH      1
```

```
#define APP_PAYLOAD_LENGTH2        1800 //100 //

#define NODE5_TOGGLE_CMD         9
#define NODE5_SEND_DATA_CMD      10
#define SENSOR5_REPORT_CMD       11

// Application in ADC Sampling

//#define NUMBER_OF_SAMPLES 250 //  Maximum 90%of 8KB SRAM == 7500 Data
#define NUMBER_OF_SAMPLES 300  //1200 //  3 CH Maximum NUMBER_OF_SAMPLES ==
6000 Data

UINT16 adcValues1[3*NUMBER_OF_SAMPLES];
//UINT16 adcValues2[3*NUMBER_OF_SAMPLES];
UINT8 tempH;
UINT8 tempL;
UINT16 i=0;


/*********************************************************************************
* LOCAL VARIABLES
*/
static UINT8 TxDataBuffer_main[APP_PAYLOAD_LENGTH]; // Coordinator
static UINT8 RxDataBuffer_main[APP_PAYLOAD_LENGTH2]; // Coordinator


static UINT8 TxDataBuffer2_node5[APP_PAYLOAD_LENGTH]; // Sensor
static UINT8 TxDataBuffer_node5[APP_PAYLOAD_LENGTH2]; // Sensor
static UINT8 RxDataBuffer_node5[APP_PAYLOAD_LENGTH]; // Sensor
static UINT8 RxDataBuffer2_node5[APP_PAYLOAD_LENGTH]; // Sensor




static basicRfCfg_t basicRfConFigure;


#ifdef SECURITY_CCM
// Security key
static uint8 key[]= {
   0xc0, 0xc1, 0xc2, 0xc3, 0xc4, 0xc5, 0xc6, 0xc7,
   0xc8, 0xc9, 0xca, 0xcb, 0xcc, 0xcd, 0xce, 0xcf,
};
#endif

/*********************************************************************************
* LOCAL FUNCTIONS
*/
static void appNode5();

/*************************************************************************
```

```
* @fn  dmaChannel_3  ---->  For transmitting Out
*****************************************************************************/
//Setting up the DMA  Channel_3 For &adcValues1 --> UART U0DBUF.
void dmaChannel_3(void)
{
  DMA_DESC dmaChannel;

  SET_WORD(dmaChannel.SRCADDRH, dmaChannel.SRCADDRL,
&adcValues1[0]);//0xFE00);//&adcValues1);//0xF000);// // The start address of the data to be
transmitted
  SET_WORD(dmaChannel.DESTADDRH, dmaChannel.DESTADDRL, &X_U0DBUF);
//&X_RFD); //// destString); // The start address of the destination.
  SET_WORD(dmaChannel.LENH, dmaChannel.LENL, sizeof(adcValues1));    // Setting the
number of bytes to transfer.
  dmaChannel.VLEN      = VLEN_USE_LEN;  // Using the length field to determine how many
bytes to transfer.
  dmaChannel.PRIORITY  = PRI_LOW;   // PRI_LOW; // // High priority.
  dmaChannel.M8        = M8_USE_8_BITS; // Irrelevant since length is determined by the
LENH and LENL.
  dmaChannel.IRQMASK   = FALSE; //FALSE;  // TRUE;      // The DMA shall not issue an IRQ
upon completion.
  dmaChannel.DESTINC   = DESTINC_0;     // The destination address is to be incremented by
0 after each transfer.
  dmaChannel.SRCINC    = SRCINC_1;      // The source address incremented by 1 byte after
each transfer.
  dmaChannel.TRIG      = 15;//DMATRIG_NONE;  // The DMA channel will be started manually.
  dmaChannel.TMODE     = TMODE_SINGLE;//_REPEATED;   // The number of bytes
specified by LENH and LENL is transferred.
  dmaChannel.WORDSIZE  = WORDSIZE_BYTE; // One byte is transferred each time.


  // Setting where the DMA channel is to read the desciptor and arming the DMA channel.
  DMA_SET_ADDR_DESC1234(&dmaChannel);
  DMA_ABORT_CHANNEL(1);
  DMA_ARM_CHANNEL(1);

  halWait(0xFF);
  halWait(0xFF);


  // Enable DMA interrupt and Clear potential pending DMA interrupt requests
  //IEN0 |= 0x80; IEN1 |= 0x01;  IRCON &= ~0x01;
  //   DMAIRQ = 0x00;

  // Send the very first UART byte to trigger a UART TX session
  i = 0xCDAB;
  U0DBUF = i;//adcValues1[0];



//    halLedSet(3);
```

```
  TxDataBuffer2_node5[0] = SENSOR5_REPORT_CMD; // Start SENSOR-Reading Command
  basicRfSendPacket(SWITCH_ADDR, TxDataBuffer2_node5, APP_PAYLOAD_LENGTH);
  halLedSet(3);


  basicRfReceiveOn();
  while(!basicRfPacketIsReady());

  if(basicRfReceive(RxDataBuffer2_node5, APP_PAYLOAD_LENGTH, NULL)>0) {
    if(RxDataBuffer2_node5[0] == NODE5_SEND_DATA_CMD)
        {


  memcpy(TxDataBuffer_node5,adcValues1,sizeof(TxDataBuffer_node5)); // Start Transmitting
Data

  for(i=0;i<=18;i++)
  {
    basicRfSendPacket(SWITCH_ADDR, &TxDataBuffer_node5[i*100],
100);//APP_PAYLOAD_LENGTH2);
  }

        halLedClear(1);

        }

  }

//   halLedClear(1);

}// End of  DMA Channel 3; transfer &adcValues1 --> U0DBUF

/*****************************************************************************
* @fn          appLight/Sensor
*
* @brief       Application code for light application. Puts MCU in endless
*              loop waiting for user input from joystick.
*
* @param       basicRfConFigure - file scope variable. Basic RF configuration data
*              RxDataBuffer_node - file scope variable. Pointer to buffer for RX data
*
* @return      none
*/
static void appNode5()
{

  // Initialize BasicRF
    basicRfConFigure.myAddr = NODE5_ADDR;

    if(basicRfInit(&basicRfConFigure)==FAILED) {
      HAL_ASSERT(FALSE);
```

```
    }
    basicRfReceiveOn();



    // Main loop
    while (TRUE) {

      while(!basicRfPacketIsReady());
      if(basicRfReceive(RxDataBuffer_node5, APP_PAYLOAD_LENGTH, NULL)>0) {
        if(RxDataBuffer_node5[0] == NODE5_TOGGLE_CMD)
        {
//            halLedToggle(3);

//**********   Start Sampling ADC conversion*****************************


   memset(adcValues1, 1, sizeof(adcValues1));

   //*************************************************************************
   // Setting up the DMA  Channel0 For &X_ADCH --> &adcValues10

     DMA_DESC dmaAdc0;

     SET_WORD(dmaAdc0.SRCADDRH, dmaAdc0.SRCADDRL,   &X_ADCL);
     SET_WORD(dmaAdc0.DESTADDRH, dmaAdc0.DESTADDRL,
(&adcValues1));//0xFE00);//&adcValues10);//0xF000);//
     SET_WORD(dmaAdc0.LENH, dmaAdc0.LENL,NUMBER_OF_SAMPLES);//1;
     dmaAdc0.VLEN         = VLEN_USE_LEN;
     dmaAdc0.PRIORITY     = PRI_HIGH;
     dmaAdc0.M8           = M8_USE_8_BITS;
     dmaAdc0.IRQMASK      = TRUE;// TRUE;//
     dmaAdc0.DESTINC      = DESTINC_1;
     dmaAdc0.SRCINC       = SRCINC_0;
     dmaAdc0.TRIG         = 28;
     dmaAdc0.TMODE        = TMODE_SINGLE;//_REPEATED;//;//
     dmaAdc0.WORDSIZE     = WORDSIZE_WORD;

     // Setting the descriptor pointer and arming the DMA. Using DMA channel 0
     DMA_SET_ADDR_DESC0(&dmaAdc0);
     DMA_ARM_CHANNEL(0);

   //*************************************************************************
   // Setting up timer 1 to generate sampling commands to the ADC.
   // Note 1 clock in Period = 1 microsecond
     TIMER1_INIT();
//     halSetTimer1Period(40000); // Sampling at 25Hz
//      halSetTimer1Period(10000); // Sampling at 100Hz
//      halSetTimer1Period(2000); // Sampling at 500Hz
//     halSetTimer1Period(1000);// Sampling at 1kHz
       halSetTimer1Period(500);// Sampling at 2kHz
//     halSetTimer1Period(200);// Sampling at 5kHz
```

```
//      halSetTimer1Period(167);// Sampling at 6kHz

    T1CCTL0 = 0x24;

  //*************************************************************************
  // Starting timer 1
    TIMER1_RUN(TRUE);

  //*************************************************************************
  // Setting up the ADC to sample from channel 7 (pin P0.7 pot meter)

    ADC_ENABLE_CHANNEL(7);
    ADC_SEQUENCE_SETUP(ADC_REF_AVDD | ADC_14_BIT | ADC_AIN7);
    ADC_TRIGGER_FROM_TIMER1();

  // wait until finish DMA
    while((DMAIRQ & 0x01) == 0x00);
 //   ADC_DISABLE_CHANNEL(7);

//*************************************************************************
  // Setting up the DMA  Channel1 For &X_ADCH --> &adcValues11
    DMA_DESC dmaAdc1;

    SET_WORD(dmaAdc1.SRCADDRH, dmaAdc1.SRCADDRL,   &X_ADCL);
    SET_WORD(dmaAdc1.DESTADDRH, dmaAdc1.DESTADDRL,
(&adcValues1[0]+NUMBER_OF_SAMPLES));//0xFE00);//&adcValues11);//0xF000);//

    SET_WORD(dmaAdc1.LENH, dmaAdc1.LENL,NUMBER_OF_SAMPLES);//1;
    dmaAdc1.VLEN         = VLEN_USE_LEN;
    dmaAdc1.PRIORITY     = PRI_HIGH;//LOW;
    dmaAdc1.M8           = M8_USE_8_BITS;
    dmaAdc1.IRQMASK      = TRUE;//FALSE;//
    dmaAdc1.DESTINC      = DESTINC_1;
    dmaAdc1.SRCINC       = SRCINC_0;
    dmaAdc1.TRIG         = 27;//27;
    dmaAdc1.TMODE        = TMODE_SINGLE_REPEATED;//;//
    dmaAdc1.WORDSIZE     = WORDSIZE_WORD;
    // Setting the descriptor pointer and arming the DMA. Using DMA channel 1
    DMA_SET_ADDR_DESC1234(&dmaAdc1);
    DMA_ARM_CHANNEL(1);
    //i = (&adcValues1[0]);
  //*************************************************************************
  // Setting up the ADC to sample from channel 6 (pin P0.6 pot meter)
    ADC_ENABLE_CHANNEL(6);
    ADC_SEQUENCE_SETUP(ADC_REF_AVDD | ADC_14_BIT | ADC_AIN6);


  // wait until finish DMA
    while((DMAIRQ & 0x02) == 0x00);
    DMAIRQ &= 0x00;

 //    ADC_DISABLE_CHANNEL(6);
```

```
  //***************************************************************************
  // Setting up the DMA  Channel1 For &X_ADCH --> &adcValues12
     DMA_DESC dmaAdc2;

     SET_WORD(dmaAdc2.SRCADDRH, dmaAdc2.SRCADDRL,   &X_ADCL);
     SET_WORD(dmaAdc2.DESTADDRH, dmaAdc2.DESTADDRL,
(&adcValues1[0]+2*NUMBER_OF_SAMPLES));//0xFE00);//&adcValues12);//0xF000);//
     SET_WORD(dmaAdc2.LENH, dmaAdc2.LENL,NUMBER_OF_SAMPLES);//1;
     dmaAdc2.VLEN          = VLEN_USE_LEN;
     dmaAdc2.PRIORITY      = PRI_LOW;
     dmaAdc2.M8            = M8_USE_8_BITS;
     dmaAdc2.IRQMASK       = TRUE;//FALSE;// TRUE;//
     dmaAdc2.DESTINC       = DESTINC_1;
     dmaAdc2.SRCINC        = SRCINC_0;
     dmaAdc2.TRIG          = 26;
     dmaAdc2.TMODE         = TMODE_SINGLE;//_REPEATED;//;//
     dmaAdc2.WORDSIZE      = WORDSIZE_WORD;

     // Setting the descriptor pointer and arming the DMA. Using DMA channel 0
     DMA_SET_ADDR_DESC1234(&dmaAdc2);
     DMA_ABORT_CHANNEL(1);
     DMA_ARM_CHANNEL(1);

     //***************************************************************************
  // Setting up the ADC to sample from channel 5 (pin P0.5 pot meter)
     ADC_ENABLE_CHANNEL(5);
     ADC_SEQUENCE_SETUP(ADC_REF_AVDD | ADC_14_BIT | ADC_AIN5);
// wait until finish DMA
     //while((DMAIRQ & 0x04) == 0x00);

  // Main loop
   while (1)       // Push S1 @ P1_0 to STOP Application
   {
     // Checking if a DMA transfer has been performed.
     // Note: DMA_CHANNEL_1 = 0x02

        if((DMAIRQ & DMA_CHANNEL_1)==0x02)
        {
          for(i=0;i<=3*NUMBER_OF_SAMPLES-1;i++)
          {
              tempH = adcValues1[i] ;
              tempL = adcValues1[i]>>8;
             // adcValues1[i] = 0xAA;
              adcValues1[i] = tempL;
              adcValues1[i] |= tempH << 8;
              adcValues1[i] >>= 4;   //remove 4 bit from 16 bit-> 12bit ADC
//              adcValues1[i] >>= 8;   //remove 4 bit from 16 bit-> 8bit ADC

          }
```

```
          DMAIRQ &= ~0x07; //reset interrupt bit
          dmaChannel_3();
//          halLedSet(3);   //turn on LED 1


        }// End of  DMA transfer &adcValues1 --> UART U0DBUF.
   }// End of while(1)

   }//End of NODE2_TOGGLE_CMD
   }//End of basicRfReceive Node2


//*************************************************************************
//*************************************************************************
  }//End of while(true)
} //End of AppNode3


/*************************************************************************************
* @fn          main
*
* @brief       This is the main entry of the "Light Switch" application.
*              After the application modes are chosen the switch can
*              send toggle commands to a light device.
*
* @param       basicRfConFigure - file scope variable. Basic RF configuration
*              data
*              appState - file scope variable. Holds application state
*
* @return      none
*/

void main(void)
{
//    uint8 appMode = NONE;

    // ConFigure basicRF
    basicRfConFigure.panId = PAN_ID;
    basicRfConFigure.channel = RF_CHANNEL;
    basicRfConFigure.ackRequest = TRUE;
#ifdef SECURITY_CCM
    basicRfConFigure.securityKey = key;
#endif



// Initalise board peripherals
//    P0SEL = 0x00; //Ú
//    P0DIR = 0x1C; //
//    P0_2 = 0;

    halBoardInit();
```

```
   halJoystickInit();

   // Initalise hal_rf
   if(halRfInit()==FAILED) {
      halLedSet(1);
     HAL_ASSERT(FALSE);

   }

   // Indicate that device is powered
   halLedSet(1);

   // Wait for user to press S1 to enter menu  at Port 1_0
//    while (halButtonPushed()!=HAL_BUTTON_1);
//    halLedSet(3);
   halMcuWaitMs(350);


//******************Selecting Mode for Operation  ******************************
// Transmitter application

//    appSwitch();//   #1 Coordinator

// Receiver application
   appNode5();//   #2  Sensor



// Role is undefined. This code should not be reached
   HAL_ASSERT(FALSE);


}



//*****************************************************************************************
```

A.2

Source code of Programming the ZigBee PAN network coordinator

```
//*****************************************************************************
  Filename: SensorCollector_12bit_3CH.c

Target:       cc2430
Author:       Suratsavadee K.
Revised:      June 2009


  Description:  This application function either as a Coordinator/Sensor
  The role of the application is chosen within this program/sourcecode at initialisation.

  Push S1 At Coordinator -->  Sensor Start Sampling
  LED 1 (Both Coordinator/Sensor) indicates that device is powered.
  LED 2 (Sensor) indicates at the end of ADC conversion.
*****************************************************************************/

/*****************************************************************************
* INCLUDES
*/
//#include <hal_lcd.h>
#include <hal_led.h>
#include <hal_joystick.h>
#include <hal_assert.h>
#include <hal_board.h>
#include <hal_int.h>
#include "hal_mcu.h"
#include "hal_button.h"
#include "hal_rf.h"
#include "util_lcd.h"
#include "basic_rf.h"

#include "app_ex.h"
#include <string.h>
#include <stdio.h>

/*****************************************************************************
* CONSTANTS
*/
// Application parameters
#define RF_CHANNEL              25      // 2.4 GHz RF channel

// BasicRF address definitions
#define PAN_ID              0x2007
#define SWITCH_ADDR         0x2510


#define NODE2_ADDR          0x2520
#define NODE3_ADDR          0x2530
```

```
#define NODE4_ADDR          0x2540
#define NODE5_ADDR          0x2550

#define APP_PAYLOAD_LENGTH       1
#define APP_PAYLOAD_LENGTH2       1800//   1500 //100 //

#define NODE2_TOGGLE_CMD        0
#define SENSOR2_REPORT_CMD       1
#define NODE2_SEND_DATA_CMD      2


#define NODE3_TOGGLE_CMD        3
#define NODE3_SEND_DATA_CMD      4
#define SENSOR3_REPORT_CMD       5

#define NODE4_TOGGLE_CMD        6
#define NODE4_SEND_DATA_CMD      7
#define SENSOR4_REPORT_CMD       8



#define NODE5_TOGGLE_CMD        9
#define NODE5_SEND_DATA_CMD      10
#define SENSOR5_REPORT_CMD       11


// Application in ADC Sampling

//#define NUMBER_OF_SAMPLES 250 //  Maximum 90%of 8KB SRAM == 7500 Data
#define NUMBER_OF_SAMPLES 300  //1200 //  3 CH Maximum NUMBER_OF_SAMPLES ==
6000 Data

//UINT16 adcValues1[3*NUMBER_OF_SAMPLES];
UINT16 adcValues2[3*NUMBER_OF_SAMPLES];
UINT16 adcValues3[3*NUMBER_OF_SAMPLES];
UINT8 tempH;
UINT8 tempL;
UINT16 i=0;


/*********************************************************************************
* LOCAL VARIABLES
*/
static UINT8 TxDataBuffer_main[APP_PAYLOAD_LENGTH];// Coordinator

static UINT8 RxDataBuffer_main[APP_PAYLOAD_LENGTH2];// Coordinator


static UINT8 RxDataBuffer_main2[APP_PAYLOAD_LENGTH];// Coordinator
static UINT8 RxDataBuffer_main3[APP_PAYLOAD_LENGTH]; // Coordinator

static basicRfCfg_t basicRfConFigure;
```

```
#ifdef SECURITY_CCM
// Security key
static uint8 key[]= {
    0xc0, 0xc1, 0xc2, 0xc3, 0xc4, 0xc5, 0xc6, 0xc7,
    0xc8, 0xc9, 0xca, 0xcb, 0xcc, 0xcd, 0xce, 0xcf,
};
#endif

/*********************************************************************************
* LOCAL FUNCTIONS
*/

static void appSwitch();

/*********************************************************************************
* @fn  initUART
*********************************************************************************/
void initUART(void)
{
  IO_PER_LOC_UART0_AT_PORT1_PIN2345();
//   UART_SETUP(0, 57600, HIGH_STOP);
  UART_SETUP(0, 9600, HIGH_STOP);
  UTX0IF = 1;

}

/*********************************************************************************
* @fn  dmaChannel_4  ---->  For Coordinator Receiving Data
*********************************************************************************/
//Setting up the DMA  Channel_3 For &adcValues1 --> UART U0DBUF.  DMA trig NO19
void dmaChannel_4(void)
{
  DMA_DESC dmaChannel;

  SET_WORD(dmaChannel.SRCADDRH, dmaChannel.SRCADDRL, &adcValues2[0]);//&X_RFD);  //   //0xFE00);//&adcValues1);//0xF000);// // The start address of the data to be transmitted
//                SET_WORD(dmaChannel.SRCADDRH, dmaChannel.SRCADDRL, &adcValues3[0]);//&X_RFD); //  //


  SET_WORD(dmaChannel.DESTADDRH, dmaChannel.DESTADDRL, &X_U0DBUF); // destString); // The start address of the destination.
  SET_WORD(dmaChannel.LENH, dmaChannel.LENL, sizeof(adcValues2));      // Setting the number of bytes to transfer.
  dmaChannel.VLEN       = VLEN_USE_LEN;  // Using the length field to determine how many bytes to transfer.
  dmaChannel.PRIORITY  = PRI_LOW;   // PRI_LOW; // // High priority.
  dmaChannel.M8          = M8_USE_8_BITS; // Irrelevant since length is determined by the LENH and LENL.
```

```
  dmaChannel.IRQMASK   = FALSE; //FALSE;  // TRUE;      // The DMA shall not issue an IRQ
upon completion.
  dmaChannel.DESTINC   = DESTINC_0;     // The destination address is to be incremented by
0 after each transfer.
  dmaChannel.SRCINC    = SRCINC_1;      // The source address incremented by 1 byte after
each transfer.
  dmaChannel.TRIG      = 15;//DMATRIG_NONE;  // The DMA channel will be started manually.
  dmaChannel.TMODE          = TMODE_SINGLE;//_REPEATED;      // The number of bytes
specified by LENH and LENL is transferred.
  dmaChannel.WORDSIZE  = WORDSIZE_BYTE; // One byte is transferred each time.


  // Setting where the DMA channel is to read the desciptor and arming the DMA channel.
  DMA_SET_ADDR_DESC1234(&dmaChannel);
  DMA_ABORT_CHANNEL(1);
  DMA_ARM_CHANNEL(1);

  halWait(0xFF);
  halWait(0xFF);


  // Enable DMA interrupt and Clear potential pending DMA interrupt requests
  //IEN0 |= 0x80; IEN1 |= 0x01;  IRCON &= ~0x01;
  //   DMAIRQ = 0x00;

  // Send the very first UART byte to trigger a UART TX session
  i = 0xCDAB;
  U0DBUF = i;//adcValues1[0];

//  halLedSet(3);
//halLedClear(1);

}// End of  DMA Channel , transfer &adcValues1 --> U0DBUF

//*****************************************************************************
/*****************************************************************************
* @fn          appSwitch/Coordinator
*
* @brief       Application code for switch application. Puts MCU in
*              endless loop to wait for commands from from switch
*
* @param       basicRfConFigure - file scope variable. Basic RF configuration data
*              TxDataBuffer_main - file scope variable. Pointer to buffer for TX
*              payload
*              appState - file scope variable. Holds application state
*
* @return      none
*/
static void appSwitch()
{

//   memset(adcValues2, 5, sizeof(adcValues2));
```

```
//   memset(adcValues3, 9, sizeof(adcValues3));

   initUART();


    // Initialize BasicRF
    basicRfConFigure.myAddr = SWITCH_ADDR;

    if(basicRfInit(&basicRfConFigure)==FAILED) {
      HAL_ASSERT(FALSE);
    }

//;
    // Main loop


    while (1) {


     if (halButtonPushed())
{     // S1_P1_0 halButtonPushed

// NOTE  This is IMPORTANT POINT WE NEED TO CONSIDER THE SEQUENC OF DATA
//

         TxDataBuffer_main[0] = NODE5_TOGGLE_CMD; // Start Sampling Command
         basicRfSendPacket(NODE5_ADDR, TxDataBuffer_main, APP_PAYLOAD_LENGTH);


         TxDataBuffer_main[0] = NODE4_TOGGLE_CMD; // Start Sampling Command
         basicRfSendPacket(NODE4_ADDR, TxDataBuffer_main, APP_PAYLOAD_LENGTH);

         TxDataBuffer_main[0] = NODE3_TOGGLE_CMD; // Start Sampling Command
         basicRfSendPacket(NODE3_ADDR, TxDataBuffer_main, APP_PAYLOAD_LENGTH);


         TxDataBuffer_main[0] = NODE2_TOGGLE_CMD; // Start Sampling Command
         basicRfSendPacket(NODE2_ADDR, TxDataBuffer_main, APP_PAYLOAD_LENGTH);



//*******************************
// ************ Last Channel of Sampling Channel need to acknowledge the Coordinator

         //  Note Read Correct

        basicRfReceiveOn();
        while(!basicRfPacketIsReady());

        if(basicRfReceive(RxDataBuffer_main2, APP_PAYLOAD_LENGTH, NULL)>0) {
           if(RxDataBuffer_main2[0] == SENSOR4_REPORT_CMD)
           {
```

```
            halLedSet(3);
//        halLedClear(1);
          }
          }

/*
       if(basicRfReceive(RxDataBuffer_main3, APP_PAYLOAD_LENGTH, NULL)>0) {
          if(RxDataBuffer_main3[0] == SENSOR3_REPORT_CMD)
          {
            halLedSet(1);
//        halLedClear(1);
          }
          }

*/



     }//End of ButtonPushed


//*************************************************************


 //************   Receive Data from Node 5**********************************

    while (halButtonPushed2())  // Pushed2_P1_7
      { // S3_P1_3 halButtonPushed3


       TxDataBuffer_main[0] = NODE5_SEND_DATA_CMD; // Start Sampling Command
       basicRfSendPacket(NODE5_ADDR, TxDataBuffer_main, APP_PAYLOAD_LENGTH);
//       halLedClear(3);

       basicRfReceiveOn();
//       while(!basicRfPacketIsReady());

              for(i=0;i<=18;i++)
              {
              while(!basicRfPacketIsReady());

              basicRfReceive(&RxDataBuffer_main[i*100],                                    100,
NULL);//APP_PAYLOAD_LENGTH2);

memcpy(&adcValues2[i*50],&RxDataBuffer_main[i*100],100);//sizeof(RxDataBuffer_node));
              } //End of for

//          halLedSet(3);
         dmaChannel_4();
//          halLedClear(3);
//          halLedClear(1);
```

```
          halLedSet(1);
          halLedSet(3);
          halLedSet(5);


       }  //End of halButtonPushed3


//*****************************************************************************
 //************   Receive Data from Node 4 **********************************

    while (halButtonPushed6())  // Pushed6  P1_6
       { // S3_P1_3 halButtonPushed3


        TxDataBuffer_main[0] = NODE4_SEND_DATA_CMD; // Start Sampling Command
        basicRfSendPacket(NODE4_ADDR, TxDataBuffer_main, APP_PAYLOAD_LENGTH);
//        halLedClear(3);

        basicRfReceiveOn();
//        while(!basicRfPacketIsReady());

                for(i=0;i<=18;i++)
                {
                while(!basicRfPacketIsReady());
 //      halLedSet(5);
                basicRfReceive(&RxDataBuffer_main[i*100],                                    100,
NULL);//APP_PAYLOAD_LENGTH2);

memcpy(&adcValues2[i*50],&RxDataBuffer_main[i*100],100);//sizeof(RxDataBuffer_node));
                } //End of for

//          halLedSet(3);
          dmaChannel_4();

          halLedClear(3);
          halLedClear(1);
          halLedSet(5);

       }  //End of halButtonPushed3


//*****************************************************************************
//************   Receive Data from Node 3 **********************************

   while (halButtonPushed4())  // Pushed4_P0_0
      { // S3_P1_3 halButtonPushed3
```

```
        TxDataBuffer_main[0] = NODE3_SEND_DATA_CMD; // Start Sampling Command
        basicRfSendPacket(NODE3_ADDR, TxDataBuffer_main, APP_PAYLOAD_LENGTH);


        basicRfReceiveOn();
//        while(!basicRfPacketIsReady());

                for(i=0;i<=18;i++)
                {
                while(!basicRfPacketIsReady());
//       halLedSet(5);
                basicRfReceive(&RxDataBuffer_main[i*100],                                100,
NULL);//APP_PAYLOAD_LENGTH2);

memcpy(&adcValues2[i*50],&RxDataBuffer_main[i*100],100);//sizeof(RxDataBuffer_node));
                } //End of for

//          halLedSet(3);
          dmaChannel_4();

          halLedClear(1);
          halLedClear(5);

          halLedSet(3);

       }  //End of halButtonPushed4



//*************************************************************************

 //************   Receive Data from Node 2 **********************************

     while (halButtonPushed5())  // Pushed5_P0_1
      { // S3_P1_3 halButtonPushed3


        TxDataBuffer_main[0] = NODE2_SEND_DATA_CMD; // Start Sampling Command
        basicRfSendPacket(NODE2_ADDR, TxDataBuffer_main, APP_PAYLOAD_LENGTH);


        basicRfReceiveOn();
//        while(!basicRfPacketIsReady());

                for(i=0;i<=18;i++)
                {
                while(!basicRfPacketIsReady());

                basicRfReceive(&RxDataBuffer_main[i*100],                                100,
NULL);//APP_PAYLOAD_LENGTH2);
```

```
memcpy(&adcValues2[i*50],&RxDataBuffer_main[i*100],100);//sizeof(RxDataBuffer_node));
                } //End of for


          dmaChannel_4();

          halLedClear(3);
          halLedClear(5);
          halLedSet(1);

       }  //End of halButtonPushed5
//*****************************************************************************

//    halLedSet(5);

  }  //End of while (true)

}//End of AppSwitch

//*****************************************************************************

/*****************************************************************************
* @fn          main
*
* @brief       This is the main entry of the "Light Switch" application.
*              After the application modes are chosen the switch can
*              send toggle commands to a light device.
*
* @param       basicRfConFigure - file scope variable. Basic RF configuration
*              data
*              appState - file scope variable. Holds application state
*
* @return      none
*/

void main(void)
{
//    uint8 appMode = NONE;

   // ConFigure basicRF
   basicRfConFigure.panId = PAN_ID;
   basicRfConFigure.channel = RF_CHANNEL;
   basicRfConFigure.ackRequest = TRUE;
#ifdef SECURITY_CCM
   basicRfConFigure.securityKey = key;
#endif



// Initalise board peripherals
```

```
//    P0SEL = 0x00; //Ú
//    P0DIR = 0x1C; //
//    P0_2 = 0;

    halBoardInit();
    halJoystickInit();

    // Initalise hal_rf


    if(halRfInit()==FAILED) {
       halLedSet(1);
      HAL_ASSERT(FALSE);

    }

    // Indicate that device is powered
//    halLedSet(1);
    halLedSet(5);
//    halLedSet(3);



    halMcuWaitMs(350);


//******************Selecting Mode for Operation  ******************************
// Transmitter application

// while( !halButtonPushed3()){   // S3_P1_3 Stop Application

    appSwitch();//   #1 Coordinator

// } //End ofS1_P1_0 halButtonPushed

// Role is undefined. This code should not be reached
    HAL_ASSERT(FALSE);

}

//*****************************************************************************************
```

REFERENCES

[1] “20% wind energy by 2030: increasing wind energy’s contribution to U.S. electricity supply,” United States Department of Energy, Rep. DOE/GO-102008-2567, Jul. 2008.

[2] J. Ribrant and L. M. Bertling, “Survey of failures in wind power systems with focus on swedish wind power plants during 1997–2005”, IEEE Trans. Energy Conversion, vol. 22, no. 1, pp. 167-173, Mar. 2007.

[3] Y. Amirat, M. E. H. Benbouzid, B. Bensaker, and R. Wamkeue, “Condition monitoring and fault diagnosis in wind energy conversion systems: a review”, in Proc. 2007 IEEE International Electric Machines and Drives Conference, vol. 2, May 2007, pp. 1434-1439.

[4] M. R. Wilkinson, F. Spinato, and P. J. Tavner, “Condition monitoring of generators and other subassemblies in wind turbine drive trains”, in Proc. 2007 IEEE International Symposium on Diagnostics for Electric Machines, Power Electronics and Drives, Sep. 2007, pp. 388-392.

[5] C. A. Walford, “Wind turbine reliability: understanding and minimizing wind turbine operation and maintenance costs,” Sandia National Laboratories, Rep. SAND2006-1100, Mar. 2006.

[6] C. Hatch, “Improved wind turbine condition monitoring using acceleration enveloping,” Orbit, pp. 58-61, 2004.

[7] R. W. Hyers, J. G. McGowan, K. L. Sullivan, J. F. Manwell, and B.C. Syrett, “Condition monitoring and prognosis of utility scale wind turbines,” Energy Materials, vol. 1, no. 3. pp. 187-203, Sep. 2006.

[8] M. R. Wilkinson, F. Spianto, M. Knowles, and P. J. Tavner,“Towards the zero maintenance wind turbine,” in Proc. 41st International Universities Power Engineering Conference, vol. 1, 2006, pp.74-78.

[9] D. McMillan and G. W. Ault, “Quantification of condition monitoring benefit for offshore wind turbines,” Wind Engineering, vol. 31, no. 4, pp. 267-285, May 2007.

[10] P.J. Tavner, G.J.W. van Bussel and F. Spinato, “Machine and converter reliabilities in wind turbines,” The 3rd IET International Conference on Power Electronics, Machines and Drives, Dublin, Ireland, pp. 127-130, March 2006.

[11] Z. Hameed, Y. S. Hong, Y. M. Cho, S. H. Ahn, and C. K. Song, “Condition monitoring and fault detection of wind turbines and related algorithms: a review,” Renewable and Sustainable Energy Reviews, vol. 13, no. 1, pp. 1-39, Jan. 2009.

[12] X. Zhang, S. He, P. Zho, W. Wang, “Summerization and study of fault diagnosis technology of the main components of wind turbine generator system,” in Proc. ICSET 2008 IEEE International Conference on Sustainable Energy Technologies, Nov. 2008, pp. 1223-1226.

[13] Z. Wang and Q. Guo, “The Diagnosis method for converter fault of the variable speed wind turbine based on the neural networks”, in Proc. 2nd Int. Conf. on Innovative Computing, Information and Control, 2008.

[14] B. Lu and S. Sharma, “A literature review of IGBT fault diagnostic and protection methods for power inverters,” IEEE Trans. Industry Applications, accepted for publication, Feb. 2009. [Proc. 43rd IEEE Industrial Applications Society Annual Meeting (IAS’08), Oct. 2008, pp. 1-8].

[15] S. Durovic, S. Wiiliamson, W. Yang, and P. Tavner, “Condition monitoring artifacts for detecting winding faults in wind turbine DFIGs,” in Proc. EWEC 2009, Scientific Track – Wind Turbine Electrical Systems & Components, Marseille, France, March 16-19, 2009.

[16] O. Bennouna, N. Héraud, H. Camblong, M. Rodriguez and M. A. Kahyeh1, “Diagnosis and fault signature analysis of a wind turbine at a variable speed”, Proc. Inst. Mechanical Engineers, Part O: Journal of Risk and Reliability, vol. 223, no. 1, pp. 41-50, 2009.

[17] W. Yang, P. J. Tavner, and M. R. Wilkinson, “Condition monitoring and fault diagnosis of a wind turbine synchronous generator drive train,” IET Renewable Power Generation, vol. 3, no. 1, pp. 1-11, Mar. 2009.

[18] M. H. Hansen, “How hard can it be to pitch a wind turbine blade?” RISO Lab, Denmark Technical University. Available: www.risoe.dtu.dk/rispubl/art/2007_321_presentation.pdf.

[19] F. S. Teknik, “Advantages of hydraulic pitch control,” [Online]. Available: www.fst.dk/dyn/files/normal_items/1029-file-2/paper.pdf.

[20] W. Yang, J. Jiang, P.J. Tavner, and C.J. Crabtree, “Monitoring Wind Turbine Condition by the Approach of Empirical Mode Decomposition”, in ICEMS 2008 International Conference on Electrical Machines and Systems, Oct. 2008, pp. 736-740.

[21] T. G. Habetler, R. G. Harley, R. M. Tallam, S. B. Lee, R. Obaid, and J. Stack, “Complete current-based induction motor condition monitoring: stator, rotor, bearings, and load,” CIEP 2002 VIII IEEE International Power Electronics Congress, Oct. 2002.

[22] R. Obaid and T. G. Habetler, “Effect of load on detecting mechanical faults in small induction motors,” in Proc. 2003 Symposium on Diagnostics for Electric Machines, Power Electronics and Drives (SDEMPED), Aug 2003, pp.307-311.

[23] R. R. Schoen and T. G. Habetler, “Effects of time-varying loads on rotor fault detection in induction machines,” IEEE Trans. Industry Applications, Vol. 31, pp.900-906, July. 1995.

[24] S. A. Saleh, A. Kazzaz and G. K. Singh, “Experimental investigations on induction machines condition monitoring and fault diagnosis using digital signal processing techniques,” in 2003 Electrical Power Systems Research, pp.197-221.

[25] S. Rajagopalan, J. M. Aller, J. A. Restrepo, T. G. Habetler and R. G. Harley, “Analytic-wavelet-ridge-based detection of dynamic eccentricity in brushless direct current motors functioning under dynamic operating conditions,” IEEE Trans. Industrial Electronics, Vol. 54, No.3, pp.1410-1419, June. 2007.

[26] G. S. Maruthi and K. P. Vittal, “Electrical Fault Detection in three phase squirrel cage induction motor by vibration analysis using MEMS accelerometer,” in Proc. 2005 IEEE Power Electronics and Drive System (PEDS), pp.838-843

[27] B. McNiff, “The gearbox reliability,” in Proc. 2nd Sandia National Laboratories Wind Turbine Reliability Workshop, Sep. 2007.

[28] S. Yang, W. Li, and C. Wang, “The intelligent fault diagnosis of wind turbine gearbox based on artificial neural network,” Proc. 2008 Int. Conf. on Condition Monitoring and Diagnosis, p 1327-1330.

[29] D. J. Lekou, F. Mouzakis, A. Anastasopoulos, and D. Kourousis,“Emerging techniques for health monitoring of wind turbine gearboxes and bearings,” in Proc. EWEC 2009, Scientific Track –Operation and Maintenance, Marseille, France, March 16-19, 2009.

[30] C. Chen, C. Sun, Y. Zhang, and N. Wang, “Fault diagnosis for largescale wind turbine rolling bearing using stress wave and wavelet analysis,” in Proc. 8th Int. Conf. on Electrical Machines and Systems, vol. 3, 2005, pp. 2239-2244.

[31] L. M. Popa, B.-B. Jensen, E. Ritchie, and I. Boldea, “Condition monitoring of wind generators,” in Proc. IAS Annu. Meeting, vol. 3, 2003, pp. 1839-1846.

[32] P. Caselitz and J.Giebhardt, Advanced Maintenance and Repair for Offshore Wind Farms using Fault Prediction and Condition Monitoring Techniques (OffshoreM&R). The European Commission, DG TREN

[33] C. M. Riley, B. K. Lin, T. G. Habetler, and R. R. Schoen, “A method for sensorless on-line vibration monitoring of induction machines,” IEEE Trans. Industry Applications, Vol. 34, pp.1240-1245, Nov. 1998.

[34] Maurice L. Adamis, JR. “Rotating machinery vibration: From analysis to troubleshooting,” 2001

[35] G. S. Maruthi, and K. P. Vittal, “Electrical fault detection in three phase squairrel cage induction motor by vibration analysis using MEMS accelerometer,” in Proc. of 2005 IEEE Power Electronics and Drives Systems (PEDS), Nov. 28–30, 2005, pp. 838–843.

[36] I. F. Akyildiz, W. Su, Y. Sankarasubramaniam, and E. Cayirci, “Wireless sensor networks,” Computer Networks, vol. 38, 2002, pp. 393-422.

[37] Chipcon TI, “A True System-on-Chip solution for 2.4 GHz IEEE 802.15.4 /ZigBee® CC2430 DataSheet (Rev.2.1) http://focus.ti.com/lit/ds/symlink/ cc2430.pdf ,” 2008

[38] Analog Devices, “Small, Low Power, 3-Axis ±3 g iMEMS® Accelerometer ADXL330 datasheet (Rev. A),” 2006.

[39] S. Ondrej, B. Zdenek, F. Petr, and H. Ondrej, “Zigbee technology and device design,” in Proc. of Networking, International Conference on Systems and International Conference on Mobile Communications and Learning Technologies, Apr. 23–29, 2006, pp. 129–129.

[40] IAR Systems, “IAR Embedded Workbench IDE User Guide,” ftp://ftp.iar.se/WWWfiles/guides/ide/ouew-3.pdf, December 2004.

[41] C. Kral, T. G. Habetler, and R. G. Harley, “Detection of mechanical imbalances of induction machines without spectral analysis of time domain signal,” IEEE Trans. Industry Applications, Vol. 40, pp.1101-1106, July. 2004.

[42] W.L. Kling and J.G. Slootweg, “Wind turbines as Power Plants,” in Proceedings of the IEEE/Cigré workshop on Wind Power and the Impacts on Power Systems, 17 – 18 June 2002, Oslo, Norway.

[43] T. Burton, D. Sharpe, N. Jenkins, and E. Bossanyi, Wind Energy Handbook. John Wiley & Sons, Ltd, 2001.

[44] L. H. Hansen, L. Helle, F. Blaabjerg, E. Ritchie, S. Munk-Nielsen, H. Bindner, P. Sørensen, and B. Bak-Jensen, “Conceptual survey of generators and power electronics for wind turbines,” Risø National Laboratory, Roskilde, Denmark, Tech. Rep. Risø-R-1205(EN), ISBN 87-550-2743-8, Dec. 2001.

[45] P. Krause, O.Wasynczuk, and S. Sudhoff, Analysis of Electric Machinery and Drive Systems, 2nd ed. New York: IEEE Press, 2002.

[46] GE Wind Energy and GE Wind Turbine Brochures. [On-line] Available from http://www.gepower.com/prod_serv/products/wind_turbines/en/index.htm.

[47] R. Pena, J.C. Clare, and G. M. Asher, “Doubly fed induction generator using back-to-back PWM converters and its application to variable speed wind-energy generation,” IEE Proc.-Electr. Power Appl., Vol. 143, No 3, May 1996.

[48] R. Fadaeinedjad, M. Moallem, and G. Moschopoulos, “Simulation of a wind turbine with doubly fed induction generator by FAST and simulink,” IEEE Trans. Energy Convers., vol. 23, no. 2, pp. 690–700, Jun. 2008.

[49]F.K.A. Lima, A. Luna, P. Rodriguez, E.H. Watanabe, and F. Blaabjerg, “ Rotor Voltage Dynamics in the Doubly Fed Induction Generator During Grid Faults”, IEEE Trans. Power Electronics, vol. 25, no. 1, pp. 118-130, Jan. 2010.

[50] F. Blaabjerg and Z. Chen, Power Electronics for Modern Wind Turbines, 1st ed.. USA: Morgan & Claypool, 2006.Subir Ray, “Electrical Power System: Concept, Theory and Practice”, 2007.

BIOGRAPHICAL INFORMATION

Suratsavadee Koonlaboon Korkua received her Bachelor's and Master's degrees in Electrical Engineering from King Mongkut's Institute of Technology Ladkrabang and Chulalongkorn University, Bangkok, Thailand in 2000 and 2003 respectively. She studied control of interior permanent-magnet synchronous motors based on a fictitious permanent-Magnet flux model for her Master thesis. She worked as a lecturer in the Department of Electrical Engineering in Walailak university, Thailand during 2003-2007.

Suratsavadee Koonlaboon Korkua was a recipient of the Royal Thai Government Scholarship during 2008 to 2011. In 2008, she came to the Energy Systems Research Center (ESRC) at the University of Texas at Arlington to pursue her Ph.D. degree in Electrical Engineering. Her research interests are in the areas of condition based monitoring systems, advanced wireless sensors network (WSN) application and renewable energy technology.